

# ENGINEERING OF BIOMATERIALS

INŻYNIERIA BIOMATERIAŁÓW

JOURNAL OF POLISH SOCIETY FOR BIOMATERIALS AND FACULTY OF MATERIALS SCIENCE AND CERAMICS AGH-UST

CZASOPISMO POLSKIEGO STOWARZYSZENIA BIOMATERIAŁÓW I WYDZIAŁU INŻYNIERII MATERIAŁOWEJ I CERAMIKI AGH

**Number 167**

Numer 167

**Volume XXV**

Rocznik XXV

**Year 2022**

(Issue 4)

Rok 2022

(Zeszyt 4)

**ISSN 1429-7248**

**PUBLISHER:**

WYDAWCA:

**Polish Society  
for Biomaterials  
in Krakow**

Polskie  
Stowarzyszenie  
Biomateriałów  
w Krakowie

**EDITORIAL  
COMMITTEE:**

KOMITET  
REDAKCYJNY:

**Editor-in-Chief**

Redaktor naczelny

**Elżbieta Pamuła**

**Editor**

Redaktor

**Patrycja**

**Domalik-Pyzik**

**Secretary of editorial**

Sekretarz redakcji

**Design**

Projekt

**Katarzyna Trała**

**ADDRESS OF  
EDITORIAL OFFICE:**

ADRES REDAKCJI:

**AGH-UST**

**30/A3, Mickiewicz Av.**

**30-059 Krakow, Poland**

Akademia

Górniczno-Hutnicza

al. Mickiewicza 30/A-3

30-059 Kraków

**Issue: 250 copies**

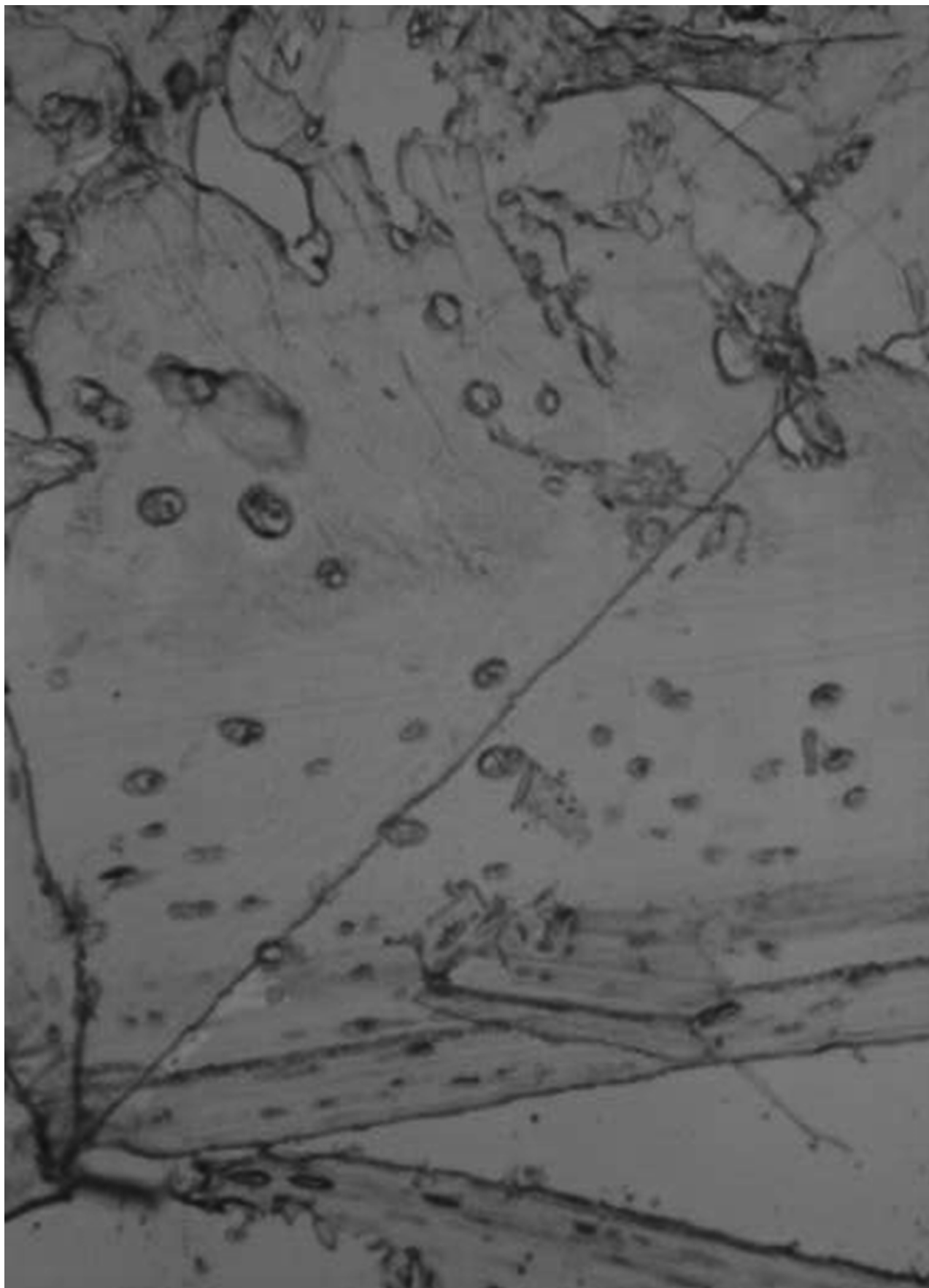
Nakład: 250 egz.

**Scientific Publishing  
House AKAPIT**

Wydawnictwo Naukowe

AKAPIT

e-mail: [wn@akapit.krakow.pl](mailto:wn@akapit.krakow.pl)



**EDITORIAL BOARD  
KOMITET REDAKCYJNY**

**EDITOR-IN-CHIEF**

Elżbieta Pamuła - AGH UNIVERSITY OF SCIENCE AND TECHNOLOGY, KRAKOW, POLAND

**EDITOR**

Patrycja Domalik-Pyzik - AGH UNIVERSITY OF SCIENCE AND TECHNOLOGY, KRAKOW, POLAND

**INTERNATIONAL EDITORIAL BOARD  
MIĘDZYNARODOWY KOMITET REDAKCYJNY**

Iulian Antoniac - UNIVERSITY POLITEHNICA OF BUCHAREST, ROMANIA

Lucie Bacakova - ACADEMY OF SCIENCE OF THE CZECH REPUBLIC, PRAGUE, CZECH REPUBLIC

Romuald Będziński - UNIVERSITY OF ZIELONA GÓRA, POLAND

Marta Błażewicz - AGH UNIVERSITY OF SCIENCE AND TECHNOLOGY, KRAKOW, POLAND

Stanisław Błażewicz - AGH UNIVERSITY OF SCIENCE AND TECHNOLOGY, KRAKOW, POLAND

Wojciech Chrzanowski - UNIVERSITY OF SYDNEY, AUSTRALIA

Jan Ryszard Dąbrowski - BIAŁYSTOK TECHNICAL UNIVERSITY, POLAND

Timothy Douglas - LANCASTER UNIVERSITY, UNITED KINGDOM

Christine Dupont - UNIVERSITÉ CATHOLIQUE DE LOUVAIN, BELGIUM

Matthias Epple - UNIVERSITY OF DUISBURG-ESSEN, GERMANY

Robert Hurt - BROWN UNIVERSITY, PROVIDENCE, USA

James Kirkpatrick - JOHANNES GUTENBERG UNIVERSITY, MAINZ, GERMANY

Ireneusz Kotela - CENTRAL CLINICAL HOSPITAL OF THE MINISTRY OF THE INTERIOR AND ADMINISTR. IN WARSAW, POLAND

Małgorzata Lewandowska-Szumieł - MEDICAL UNIVERSITY OF WARSAW, POLAND

Jan Marciniak - SILESIA UNIVERSITY OF TECHNOLOGY, ZABRZE, POLAND

Ion N. Mihailescu - NATIONAL INSTITUTE FOR LASER, PLASMA AND RADIATION PHYSICS, BUCHAREST, ROMANIA

Sergey Mikhalovsky - UNIVERSITY OF BRIGHTON, UNITED KINGDOM

Stanisław Mitura - TECHNICAL UNIVERSITY OF LIBEREC, CZECH REPUBLIC

Piotr Niedzielski - TECHNICAL UNIVERSITY OF LODZ, POLAND

Abhay Pandit - NATIONAL UNIVERSITY OF IRELAND, GALWAY, IRELAND

Stanisław Pielka - WROCLAW MEDICAL UNIVERSITY, POLAND

Vehid Salih - UCL EASTMAN DENTAL INSTITUTE, LONDON, UNITED KINGDOM

Jacek Składzień - JAGIELLONIAN UNIVERSITY, COLLEGIUM MEDICUM, KRAKOW, POLAND

Andrei V. Stanishevsky - UNIVERSITY OF ALABAMA AT BIRMINGHAM, USA

Anna Ślósarczyk - AGH UNIVERSITY OF SCIENCE AND TECHNOLOGY, KRAKOW, POLAND

Tadeusz Trzaska - UNIVERSITY SCHOOL OF PHYSICAL EDUCATION, POZNAŃ, POLAND

Dimitris Tsipas - ARISTOTLE UNIVERSITY OF THESSALONIKI, GREECE

## Wskazówki dla autorów

1. Prace do opublikowania w kwartalniku „Engineering of Biomaterials / Inżynieria Biomateriałów” przyjmowane będą wyłącznie w języku angielskim.

2. Wszystkie nadsyłane artykuły są recenzowane.

3. Materiały do druku prosimy przysyłać za pomocą systemu online ([www.biomaterials.pl](http://www.biomaterials.pl)).

4. Struktura artykułu:

• TYTUŁ • Autorzy i instytucje • Streszczenie (200-250 słów) • Słowa kluczowe (4-6) • Wprowadzenie • Materiały i metody • Wyniki i dyskusja • Wnioski • Podziękowania • Piśmiennictwo

5. Autorzy przesyłają pełną wersję artykułu, łącznie z ilustracjami, tabelami, podpisami i literaturą w jednym pliku. Artykuł w tej formie przesyłany jest do recenzentów. Dodatkowo autorzy proszeni są o przesłanie materiałów ilustracyjnych (rysunki, schematy, fotografie, wykresy) w oddzielnych plikach (format np. .jpg, .gif., .tiff, .bmp). Rozdzielczość rysunków min. 300 dpi. Wszystkie rysunki i wykresy powinny być czarno-białe lub w odcieniach szarości i ponumerowane cyframi arabskimi. W tekście należy umieścić odnośniki do rysunków i tabel.

6. Na końcu artykułu należy podać wykaz piśmiennictwa w kolejności cytowania w tekście i kolejno ponumerowany.

7. Redakcja zastrzega sobie prawo wprowadzenia do opracowań autorskich zmian terminologicznych, poprawek redakcyjnych, stylistycznych, w celu dostosowania artykułu do norm przyjętych w naszym czasopiśmie. Zmiany i uzupełnienia merytoryczne będą dokonywane w uzgodnieniu z autorem.

8. Opinia lub uwagi recenzentów będą przekazywane Autorowi do ustosunkowania się. Nie dostarczenie poprawionego artykułu w terminie oznacza rezygnację Autora z publikacji pracy w naszym czasopiśmie.

9. Za publikację artykułów redakcja nie płaci honorarium autorskiego.

10. Adres redakcji:

Czasopismo

„Engineering of Biomaterials / Inżynieria Biomateriałów”

Akademia Górniczo-Hutnicza im. St. Staszica

Wydział Inżynierii Materiałowej i Ceramiki

al. Mickiewicza 30/A-3, 30-059 Kraków

tel. (48) 12 617 44 48, 12 617 25 61

e-mail: [epamula@agh.edu.pl](mailto:epamula@agh.edu.pl), [kabe@agh.edu.pl](mailto:kabe@agh.edu.pl)

Szczegółowe informacje dotyczące przygotowania manuskryptu oraz procedury recenzowania dostępne są na stronie internetowej czasopisma:

[www.biomaterials.pl](http://www.biomaterials.pl)

## Instructions for authors

1. Papers for publication in quarterly journal „Engineering of Biomaterials / Inżynieria Biomateriałów” should be written in English.

2. All articles are reviewed.

3. Manuscripts should be submitted to editorial office through online submission system ([www.biomaterials.pl](http://www.biomaterials.pl)).

4. A manuscript should be organized in the following order:

• TITLE • Authors and affiliations • Abstract (200-250 words) • Keywords (4-6) • Introduction • Materials and Methods • Results and Discussion • Conclusions • Acknowledgements • References

5. All illustrations, figures, tables, graphs etc. preferably in black and white or grey scale should be additionally sent as separate electronic files (format .jpg, .gif., .tiff, .bmp). High-resolution figures are required for publication, at least 300 dpi. All figures must be numbered in the order in which they appear in the paper and captioned below. They should be referenced in the text. The captions of all figures should be submitted on a separate sheet.

6. References should be listed at the end of the article. Number the references consecutively in the order in which they are first mentioned in the text.

7. The Editors reserve the right to improve manuscripts on grammar and style and to modify the manuscripts to fit in with the style of the journal. If extensive alterations are required, the manuscript will be returned to the authors for revision.

8. Opinion or notes of reviewers will be transferred to the author. If the corrected article will not be supplied on time, it means that the author has resigned from publication of work in our journal.

9. Editorial does not pay author honorarium for publication of article.

10. Address of editorial office:

Journal

„Engineering of Biomaterials / Inżynieria Biomateriałów”

AGH University of Science and Technology

Faculty of Materials Science and Ceramics

30/A-3, Mickiewicz Av., 30-059 Krakow, Poland

tel. (48) 12) 617 44 48, 12 617 25 61

e-mail: [epamula@agh.edu.pl](mailto:epamula@agh.edu.pl), [kabe@agh.edu.pl](mailto:kabe@agh.edu.pl)

Detailed information concerning manuscript preparation and review process are available at the journal's website:

[www.biomaterials.pl](http://www.biomaterials.pl)





# 32<sup>nd</sup> Biomaterials in Medicine and Veterinary Medicine Annual Conference

12 – 15 October 2023 Rytro, Poland

SAVE THE DATE

12-15

OCTOBER  
2023

[www.biomat.agh.edu.pl](http://www.biomat.agh.edu.pl)



REGISTER  
AND  
SUBMIT  
AN ABSTRACT



## SPIS TREŚCI CONTENTS

<b>PHYSICAL PROPERTIES OF MATERIALS          USED FOR INFUSION SETS FOR          PHOTSENSITIVE MEDICINES</b> KAROLINA SZAFARCZYK, JANUSZ SZEWCZENKO, ERWIN MACIAK, PIOTR KAŁUŻYŃSKI, KAROLINA GOLDSZTAJN	<b>2</b>
<b>COMPOSITES BASED ON POLYVINYL          ALCOHOL, CHITOSAN, AND CURCUMIN          FOR WOUND HEALING APPLICATIONS</b> MUHAMMAD TAHIR, SILVIA VICINI, ALINA SIONKOWSKA	<b>10</b>
<b>CARTILAGE TISSUE EXAMINATION          USING ATOMIC FORCE MICROSCOPY</b> JAROSŁAW PALUCH, JAROSŁAW MARKOWSKI, JAN PILCH, WOJCIECH SMÓŁKA, KRZYSZTOF PIOTR JASIK, FILIP KILIAN, VIRGINIA LIKUS, GRZEGORZ BAJOR, DARIUSZ CHROBAK, KARSTEN GLOWKA, OLIWIA STARCZEWSKA	<b>17</b>
<b>MATERIALS BASED ON CHITOSAN          ENRICHED WITH ZINC NANOPARTICLES FOR          POTENTIAL APPLICATIONS ON THE SKIN</b> KAROLINA KULKA, ANDŻELIKA SZMEJKOWSKA, ALINA SIONKOWSKA, MAGDALENA WYPIJ, PATRYCJA GOLIŃSKA	<b>24</b>

# PHYSICAL PROPERTIES OF MATERIALS USED FOR INFUSION SETS FOR PHOTSENSITIVE MEDICINES

KAROLINA SZAFARCZYK<sup>1\*</sup> , JANUSZ SZEWCZENKO<sup>1\*</sup> ,  
ERWIN MACIAK<sup>2</sup> , PIOTR KAŁUŻYŃSKI<sup>2</sup> ,  
KAROLINA GOLDSZTAJN<sup>1</sup> 

<sup>1</sup> SILESIA UNIVERSITY OF TECHNOLOGY,  
FACULTY OF BIOMEDICAL ENGINEERING,  
DEPARTMENT OF BIOMATERIALS AND  
MEDICAL DEVICE ENGINEERING,  
40 ROOSEVELTA STR., 41-800 ZABRZE, POLAND

<sup>2</sup> SILESIA UNIVERSITY OF TECHNOLOGY,  
FACULTY OF ELECTRICAL ENGINEERING,  
DEPARTMENT OF OPTOELECTRONICS,  
2B KRZYWOSTEGO STR., 44-100 GLIWICE, POLAND

\*E-MAIL: KAROSZA926@STUDENT.POLSL.PL,  
JANUSZ.SZEWCZENKO@POLSL.PL

## Abstract

*Continuous infusion, as one of the most effective methods of delivering pharmaceuticals to patients, uses infusion pumps to which a syringe and infusion drains are connected. Photosensitive drugs that require UV-VIS protection are delivered to patients with special infusion sets that reduce harmful radiation. However, these drains have different transparencies, which can affect the success of therapy.*

*This study investigated the optical properties of two types of drains used for infusion therapy of photosensitive drugs. UV-VIS spectroscopy studies were carried out, allowing the determination of the absorbance values and absorption coefficient of the two types of drains. The spectrum of their transmittance was also analyzed. The chemical composition of the samples was tested using FTIR-ATR spectroscopy. Furthermore, the roughness and wettability parameters of the drains were determined, which affect not only the kinematics of drug flow in the drains but also the way in which light is transmitted. The results of the study can be used to propose a solution to eliminate the problem of loss of properties of the photosensitive drug in drains, in contact with light. By selecting the appropriate drain thickness, it is possible to reduce the transmission of radiation in the UV-VIS range through the drain.*

**Keywords:** infusion drains, photosensitive medicines, polyvinyl chloride, UV-VIS spectrophotometry, transmittance, absorbance

## Introduction

Medicinal products, which have been around for years in the history of mankind, are designed to reduce the effects of disease. Nowadays, where medicine and the pharmaceutical industry are developing rapidly, we have a wide range of drugs to choose from, which can prevent many diseases and even death. Not only the composition and proportions of the drug are important but also the way in which it is delivered to patients. One of the most effective methods of administering pharmaceuticals to patients is continuous infusion, which, compared to traditional gravity infusion, ensures that the preferred concentration of the drug in the blood is maintained constant, for a specified period of time. A drug product at the level of the so-called therapeutic window between the minimum therapeutic concentration and the minimum toxic concentration gives the best response of the body to the administered substance [1]. Additionally, infusion pumps are equipped with various types of alarm systems that greatly facilitate the work of medical personnel.

Some infusion drugs require special precautions during both storage and injection into the body. Particularly sensitive are photosensitive drugs, which are a group of drugs that react negatively to electromagnetic radiation in the visible and ultraviolet light range. In contact with light, they lose their physical, chemical and pharmacological properties, which can contribute to the ineffectiveness of the treatment. Moreover, their degradation products may worsen patient's condition.

Only a few studies on photosensitive pharmaceuticals and their physical and chemical transformations are available [2]. The main source of information presented on the purpose, storage, and supply of this type of drugs is the *National Register of Medicinal Products* [3] providing characteristics and brochures of selected pharmaceuticals.

Examples of photosensitive drugs are as follows: *Micafungin Accord*, *Detimedac*, *Linezolid Polpharma*. These drugs have a broad spectrum of applications. They are used in the treatment of invasive candidiasis or hospital-acquired pneumonia in both adults and newborns. They have also found use in cancer departments for the treatment of metastatic malignant melanoma, advanced *Hodgkin's disease*, or advanced soft tissue sarcomas [3].

Photosensitive drugs must be stored in the original tightly sealed packaging. Orange glass vials or special films that protect drugs from light are the most commonly used. For drug delivery, it is recommended to use light-resistant PVC infusion sets or a traditional aluminium foil-wrapped set [3]. However, it is worth paying attention to the individual components of the infusion line, which differ in translucency, as it can affect the effectiveness of the drug and thus the success of therapy.

The infusion line provides a permanent connection between the infusion pump and the patient. The syringe, the amber colored infusion extender, and the clear extension tube (FIGs. 1-3), which connects to the cannula and thus to the patient's vein, are connected to the pump in sequence. The amber syringe and the amber extension tube are adapted to protect drugs from light (FIG. 1 and FIG. 2). After a detailed review of the availability of this type of equipment and an interview with medical personnel, it can be concluded that there are no extension drains adapted for the infusion of photosensitive drugs on the global market for medical devices. In the characteristics of photosensitive drugs, it is clearly marked that infusion sets that ensure reduction of radiation transmittance are to be used.

[*Engineering of Biomaterials* 167 (2022) 2-9]

doi:10.34821/eng.biomat.167.2022.2-9

Submitted: 2023-03-22, Accepted: 2023-04-24, Published: 2023-04-30



Copyright © 2022 by the authors. Some rights reserved.  
Except otherwise noted, this work is licensed under  
<https://creativecommons.org/licenses/by/4.0>



**FIG. 1. Amber-colored syringe for infusion pumps (Polmil Company).**



**FIG. 2. Amber-colored infusion pump extension tube (Zarys Company).**



**FIG. 3. Three-way stopcock with extension tube (Zarys Company).**

During treatment, time is of the essence, and medical personnel, when trying to protect the photosensitive drug by other means, waste that time. Photosensitive drugs are used on the wards where bedridden patients require immediate and reliable treatment. That is why it is so important to make the work of doctors and nurses as efficient as possible and to ensure that there is no doubt about the effectiveness of the pharmaceutical administered.

When the materials used for the production of basic devices for injecting drugs are analyzed, it should be noted that the basic materials are polypropylene, polyethylene, and polyvinyl chloride. Typically, the syringe body is made of polypropylene (PP), while the syringe plunger is made of polyethylene (PE) [4]. The rest of the infusion line is made of poly(vinyl chloride) (PVC) [4] mixed with various additives [5].

The main purpose of the study was to determine the optical properties of the amber-colored and transparent drains used for the continuous infusion of photosensitive drugs. Their transmittance and absorbance values were compared. In addition, the chemical composition of the drains was analyzed, and the topography and wettability of their surfaces were studied.

## Materials and Methods

### Drain materials

As mentioned above, two types of materials used for the production of infusion pump drains were used for comparative studies: amber, shown in FIG. 2 and transparent, shown in FIG. 3. These drains are manufactured by Zarys. They are available from the company and are widely used in healthcare facilities.

Detailed information on the amber and transparent drain composition data was provided by the company Zarys in TABLES 1 and 2, respectively. Based on these, the main component of the drains - PVC poly(vinyl chloride) - was determined. The rest of the components are various types of additives to match the properties of the drains for processing and utility purposes. A characteristic component of the drain adapted for the infusion of photosensitive drugs is *bis(2-ethylhexyl) phenyl phosphite*, which imparts an amber color and thus increases the absorbance value of visible light radiation.

**TABLE 1. Percentage composition of the amber infusion pump extension tube.**

Substance name	Percentage composition
PVC resin	64-70%
TOTM (trioctyl trimellitate)	25-28%
ESO (epoxidized soybean oil)	4-6%
Octadecanoic acid, zinc salt	2%
Ethene, homopolymer, oxidized	1%
Bis(2-ethylhexyl) phenyl phosphite	1%

**TABLE 2. Percentage composition of the three-way stopcock with extension tube.**

Substance name	Percentage composition
PVC (polyvinylchloride polymer)	63.2%
TOTM (trioctyl trimellitate)	33.5%
Epoxidized Soybean Oil	2.3%
Calcium-Zinc based heat-stabilizer	0.6%
Lubricant	0.2%
Other components	0.2%

### FTIR-ATR Spectroscopy

A Nicolet iS50 FTIR spectrophotometer was used to study the chemical composition of the drains, together with a GladiATR Illuminate ATR measurement device. Special OMNIC software gave the possibility to read the mid-IR absorption spectra of the studied materials in the infrared range (4000-650  $\text{cm}^{-1}$ ).

Samples of each type of the drains (amber and transparent) were used in the study. The preparation of the samples required taking sections of drains approximately 7 mm in length and cutting them lengthwise (FIG. 4 and FIG. 5). The samples were studied at room temperature (25°C).

Infrared spectroscopy is a standard, fast, and economical measurement technique suitable for material characterization, e.g. polymer materials, and it provides the molecular fingerprint of the sample. It is expected that its sensitivity will enable the detection of small changes in the chemical composition of material samples related to the addition of a dye to absorb high-energy radiation in the UV-VIS range.

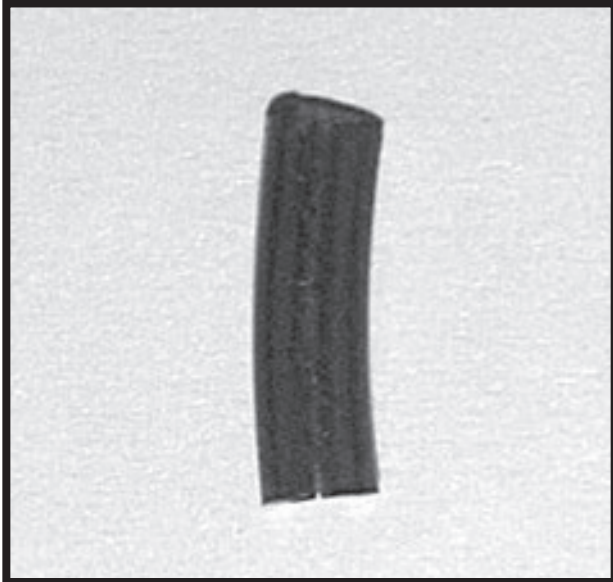


FIG. 4. Amber drain sample prepared for the FTIR-ATR spectrophotometric study.

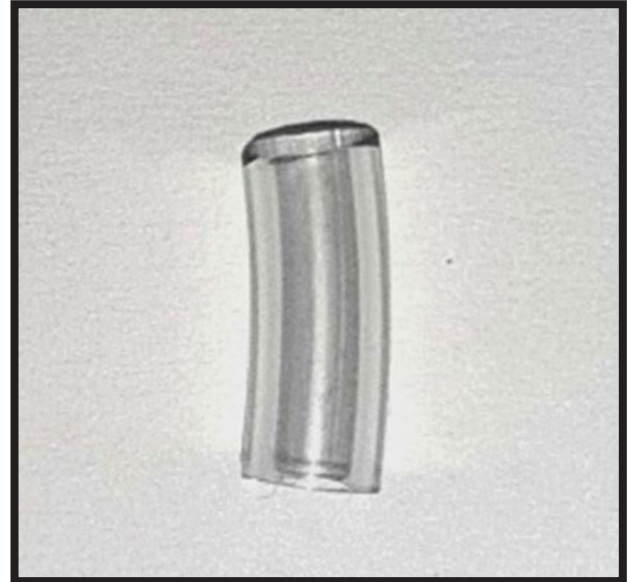


FIG. 5. Transparent drain sample prepared for the FTIR-ATR spectrophotometric study.

#### UV-VIS absorption spectroscopy

UV-VIS spectroscopy is a powerful analytical technique for determining the optical properties (transmittance, reflectance, and absorbance) of gases, liquids, and solids. It can be applied to characterize different materials, i.e. polymers and many other research and manufacturing materials. In this research, UV-VIS operated in the optical range between 300 and 800 nm. The analysis of the optical properties of the tested samples was performed based on transmittance measurements. The test stand was equipped with a deuterium tungsten light source from Ocean Optics Inc. An *Ocean Optics HR ES2000+* fiber optic spectrometer was used as a detector for the study, along with special *Ocean Optics SpectraSuite* software for viewing spectra in the range of 300-800 nm. In order to properly measure the transmittance of the samples, a system of two collimators was used in the stand so that the beam of optical radiation passing through the tested sample was collimated.

Due to the need to use flat-parallel samples in the study, steps were taken to prepare the samples for the study. The drains of each type were cut into 6 sections of approximately 7 mm in length and cut lengthwise to flatten the sample. Then, each sample was placed between two microscope slides. To ensure the flatness of the samples, metal plates with the same thickness as the walls of the drains were placed between the slides. The samples prepared in this way were heated on both sides with a heating system consisting of ceramic-tourmaline plates and a power source. The heating temperature was set at 180°C. After 3 minutes of heating, the sample still placed between the slides was left to vitrify at room temperature (FIG. 6 and FIG. 7).

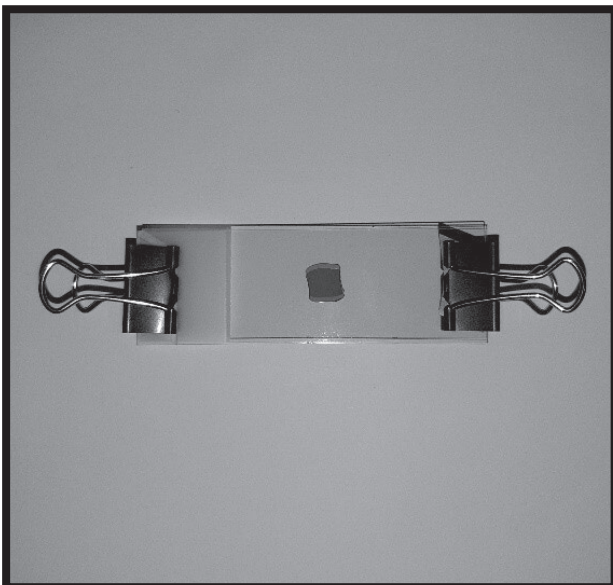


FIG. 6. Amber drain sample prepared for UV-VIS absorption spectroscopy study.

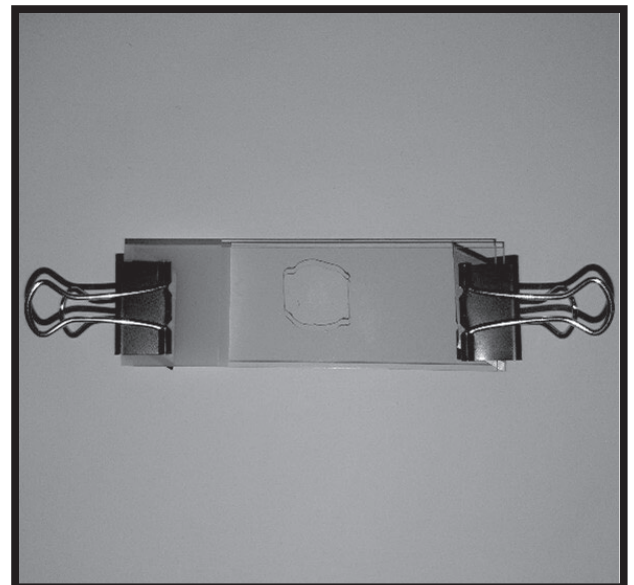


FIG. 7. Transparent drain sample prepared for UV-VIS absorption spectroscopy study.

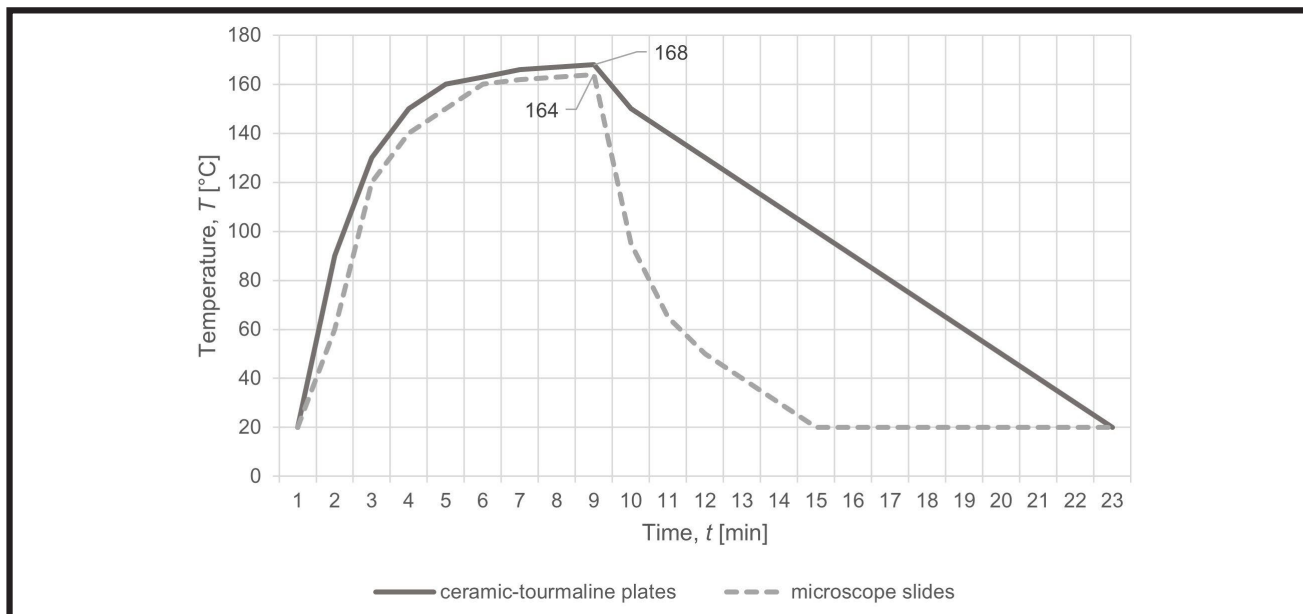


FIG. 8. Heating characteristics of the sample preparation system for UV-VIS spectrophotometric studies.

When selecting the heating temperature of the samples, the characteristic temperature ranges for PVC material were taken into consideration to prevent its degradation [6]:

- melting point  $T_m = 212^\circ\text{C}$ ,
- glass transition temperature  $T_g = 87^\circ\text{C}$ ,
- processing temperature  $T_p = 160\text{-}190^\circ\text{C}$ .

It was necessary to take into consideration the difference between the set temperature of the system and the actual temperature of heating the sample. For this purpose, the characteristics of the sample heating system were determined as a function of time (FIG. 8). The heating temperature of the plates was set within the processing temperature  $T_p = 180^\circ\text{C}$ . Using a *MY-64 multimeter of Xtreme* with a connected probe, the temperature values were measured as a function of time, both between the slides and the plates.

The temperature of the slides remains below that of the plates. A non-linear increase in temperature is observed (FIG. 8). On the other hand, when the heating system is turned off, the slides cool faster.

There is a difference in the maximum temperature value. For the measurement between the slides, it is  $4^\circ\text{C}$  lower than the measurement between the slides themselves. To reach the maximum temperature value between the microscope slides, it was necessary to wait about 9 min after turning on the heating system. After this time, the temperature oscillates around  $164^\circ\text{C}$  until the system is turned off. This temperature is the actual temperature of heating the samples and is within the range of processing temperatures.

Six samples of amber drain and one sample of transparent drain were analyzed. Each sample was sequentially placed between fiber optics. The collimated beam of radiation was directed first to the slides (as a reference measurement) and then to the sample placed between the slides. Spectral measurements must be accurate and precise representations of the target material, but there are many factors that affect the quality of spectral measurements. That is why it is so important to properly adjust the measuring system and set the appropriate parameters for recording the optical spectrum. In the measurements of the spectral transmittance of the samples, the measurements were recorded with averaging of 10 spectra. The integration time for each spectrum was 7 ms. The smoothing of the boxcar was 3. The measurements were carried out indoors with the lighting turned off.

To determine the spectral absorbance and absorption coefficients of the tested samples, the Beer-Lambert law and spectral transmittance measurements were used. Using UV-VIS spectroscopy in the spectral range of 300-800 nm, the transmittance spectra were recorded. These spectra were obtained by measuring the optical beam passing through the target samples  $I(\lambda)$  and referring it to the spectrum of the beam incident on the sample  $I_0(\lambda)$  [7]. The transmittance is defined as  $T(\lambda)$ :

$$T(\lambda) = \frac{I(\lambda)}{I_0(\lambda)} \quad (1)$$

$I_0(\lambda)$  - intensity of radiation incident on the sample (reference beam),

$I(\lambda)$  - intensity of the radiation that penetrated the sample after the absorbing layer passed through.

On the basis of transmittance measurements, the absorbance  $A(\lambda)$  of the samples was determined for peculiar spectral ranges characterized by minima in the transmittance spectrum. The absorbance  $A(\lambda)$  is the negative log-ratio of transmitted (sample in the beam) over incident (no sample in the beam) intensities:

$$A(\lambda) = -\log\left(\frac{I(\lambda)}{I_0(\lambda)}\right) = \log\left(\frac{1}{T(\lambda)}\right) \quad (2)$$

An absorption spectrum  $A(\lambda)$  shows the wavelength at which a molecule can absorb light and thus provides information about electronic state energies.

In order to quantify the absorption process in the characteristic energies of radiation, the spectral absorption coefficients of the tested samples were determined. For this purpose, the Beer-Lambert law was used, which well imitates the absorption process in poorly absorbing samples (e.g. of small thickness). Taking into account the Beer-Lambert law, the transmittance of the samples is defined as follows:

$$T(\lambda) = \frac{I(\lambda)}{I_0(\lambda)} = e^{-\alpha(\lambda)l} \quad (3)$$

$l$  - sample thickness, mm,

$\alpha$  - absorption coefficient,  $\text{mm}^{-1}$

Lambert-Beer's law shows that the intensity of a parallel beam of electromagnetic radiation decreases exponentially as the thickness of the absorbing solid increases [7]. Therefore, the absorbance  $A(\lambda)$  was given:

$$A(\lambda) = 0.4343 \cdot \alpha(\lambda)l \quad (4)$$

For spectrophotometric measurements, it is necessary to take into account the thickness of the absorbing layer  $l$ , which in the case of solids is the distance between the outer planar-parallel surfaces of the solid under study [8]. Thus, the absorption coefficient is determined as follows [8]:

$$\alpha(\lambda) = 2.302 \cdot \frac{A(\lambda)}{l} \quad (5)$$

### Thickness measurement of samples

The thickness of the samples was tested to determine the effect of heating on the thickness of the samples. For the measurements, a micrometer screw was used with an accuracy of 0.01 mm. The thickness of two types of drains was measured before and after heating.

### Surface topography studies

The study was carried out with a *Leica DCM8* optical profilometer. Using *Leica Scan* and *Leica Map Premium* software, a sample scan was obtained, profiles were extracted, and characteristic roughness parameters of the samples were determined.

Three samples of each type of the drain were prepared for the test. The roughness test requires a flat surface of the sample. For this reason, the drain samples were prepared in the same way as the samples used in UV-VIS spectrophotometric studies.

The measurement was carried out at three measuring points on both the outer and inner sides of the samples and a 20x magnification was used.

### Surface wettability studies

Four samples were selected for the wettability study. Two amber drain samples and two transparent drain samples. The samples flattened by heating were placed between two microscope slides.

For all samples, the wetting angle was measured using the sessile drop method (FIG. 9). For these measurements, a *Surftens Universal* goniometer of *OEG GmbH* was used together with the software *Surftens 4.3*. The wetting angle  $\Theta$  was measured on both the inner and outer sides of the sample, at three different measuring points.

## Results and Discussions

### FTIR-ATR Spectrophotometric studies

Based on the absorption spectra obtained (FIG. 10 and FIG. 11) there was a similarity between the studied composition of the drains and the information received by *Zarys Company*.

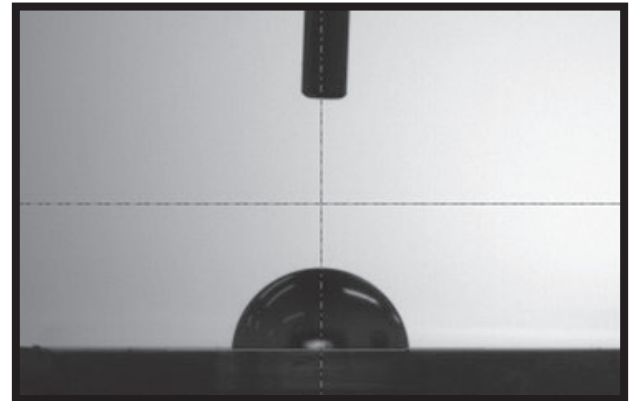


FIG. 9. Wettability study of drains by sessile drop method.

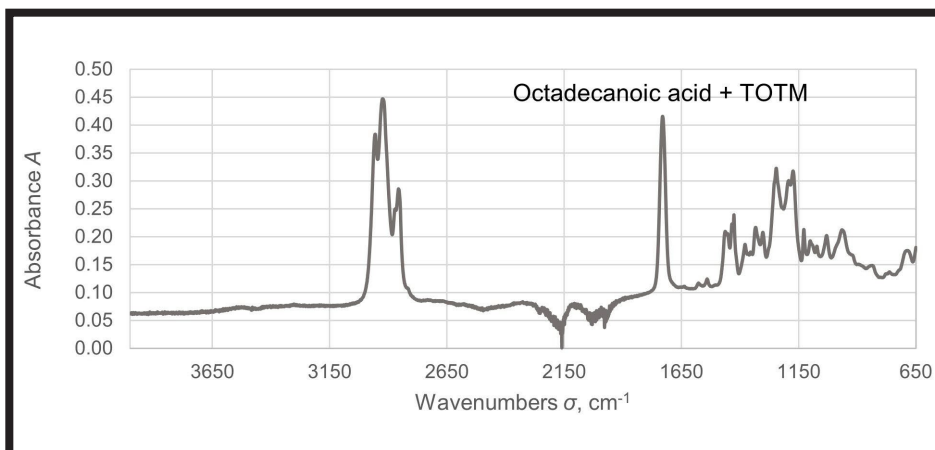


FIG. 10. FTIR-ATR absorption spectrum of the amber drain.

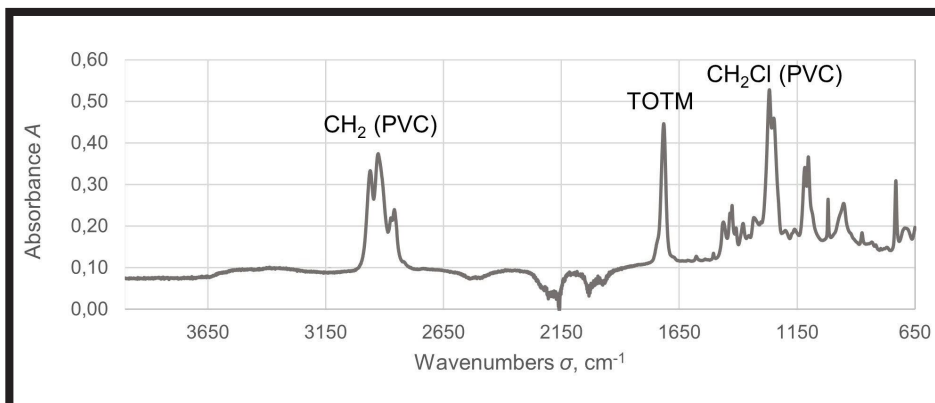


FIG. 11. FTIR-ATR absorption spectrum of the transparent drain.

The two types of drains studied overlap with the spectra of the PVC material [9]. In the vicinity of  $2900\text{ cm}^{-1}$  and  $1270\text{ cm}^{-1}$  there are signals characteristic of PVC bonds. Additionally, the presence of some plasticizers was detected. The signal near a wave number of about  $1730\text{ cm}^{-1}$  is characteristic of the plasticizer TOTM (*trioctyl trimellitate*) for both the amber and transparent drain [9,10]. For the same wavelength number, *octadecanoic acid* was detected for the amber drain [11].

The amber dye *phenyl (bis-ethylhexyl) phosphite*, as reported by the manufacturer, is present at a concentration of 1%, which may result in a small signal in the absorption spectrum. Based on the similarity of the spectra of similar compounds [12,13] it can be assumed that the absorber signal is in the region of  $1000\text{ cm}^{-1}$ . The presence of plasticizers in PVC material can be detected by vibrations in C-Cl bonds [9].

### Thickness measurement of samples

After thermal flattening of the samples, a significant difference in their thickness can be observed which may be due to different pressure force of the office clips, fluctuation of the heating temperature or variation in the heating time of the samples (TABLE 3).

### UV-VIS Spectrophotometric studies

Based on UV-VIS spectrophotometric studies, representative transmittance and absorbance spectra of the samples of two types of drains, with the same thickness, are presented (FIG. 12 and FIG. 13).

**TABLE 3. Sample thickness  $l$  with standard uncertainty before and after heating.**

Type of the drain	Thickness before heating $l$ [mm]	Average thickness after heating $l$ [mm]
Transparent drain	0.650(10)	0.373(44)
Amber drain	0.692(12)	0.348(70)

The amber color of the drain (component: *bis(2-ethylhexyl) phenyl phosphite*) causes the transmittance for both UV and VIS radiation to be limited. For radiation in the near UV range, it does not exceed 20%. For visible light, however, it increases from 450-800 nm with an inflection of the function around 550 nm but does not exceed the value of 80% for each wavelength. The lowest value of transmittance (about 0%) and thus the greatest drug safety occurs between 410-460 nm.

The lowest transmittance value (about 30%) of the transparent drain occurs at the wavelength representing ultraviolet radiation (315 nm). After that, the transmittance value increases and already at 450 nm it remains at almost 100%. From 600 nm onward, the transmittance gently decreases but remains above 96% all the time.

To compare the absorbance coefficient of the two types of drains at particular wavelengths  $\lambda$ , four characteristic points of the spectrum were chosen: 353.50 nm, 430.00 nm, 535.44 nm, 561.80 nm.

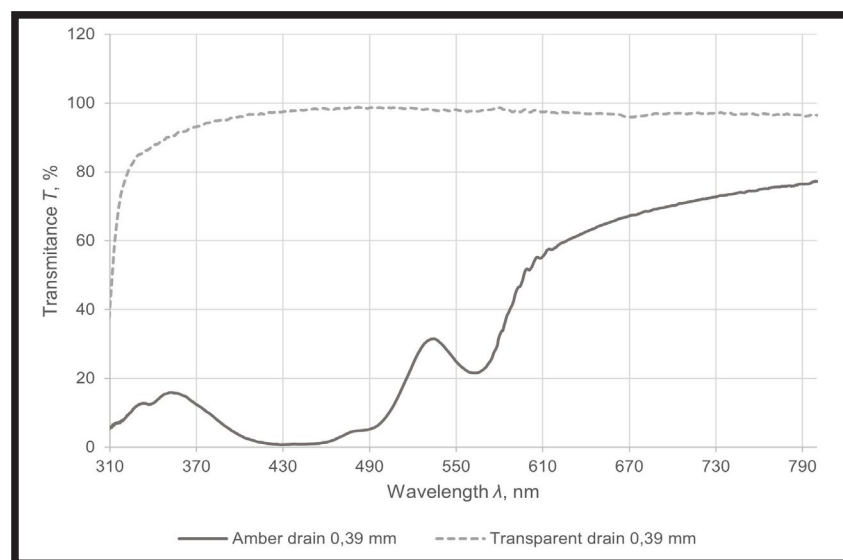


**FIG. 12. Transmittance spectra of amber sample No. 4 and transparent sample No. 1.**

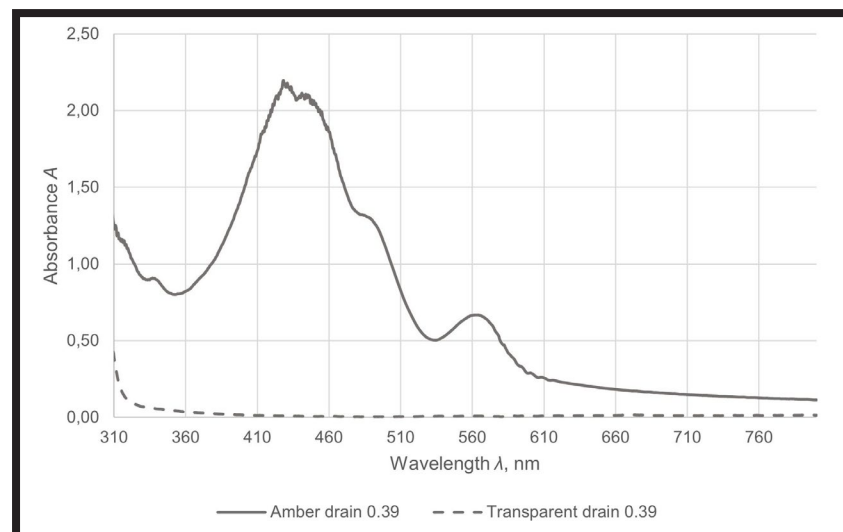


**FIG. 13. Absorbance spectra of amber sample No. 4 and transparent sample No. 1.**

**TABLE 4. Absorbance values and absorption coefficient of amber samples.**

$\lambda$ [nm]	Amber drain				Transparent drain			
	A, a.u.		1/mm		A, a.u.		1/mm	
	Range	Mean	Range	Mean	Range	Mean	Range	Mean
353.5	0.48-0.80	0.71(13)	1.92-2.19	2.05(12)	0.04-0.35	0.18(17)	0.11-0.85	0.45(39)
430.01	1.36-2.19	1.95(33)	5.20-6.18	5.66(33)	0.01-0.08	0.028(35)	0.01-0.19	0.063(85)
535.44	0.32-0.51	0.455(81)	1.20-1.47	1.317(95)	0.01-0.09	0.030(40)	0.02-0.23	0.08(10)
561.8	0.42-0.67	0.60(11)	1.60-1.92	1.73(12)	0.01-0.10	0.033(45)	0.03-0.24	0.09(10)

The tables show the calculated average values of absorbance A and absorption coefficient  $\alpha$  for the six amber samples and four transparent samples of the six tested. Transparent samples 3 and 5 were not included in the analysis of the results due to the appearance of measurement failure and the receipt of unreal results (TABLE 4).

The highest absorption coefficient of the amber drain was observed for a wavelength of 430.01 nm. For wavelengths of 535.44 nm and 561.8 nm, it occurs below  $2 \text{ mm}^{-1}$  while, for UV radiation (353.5 nm), the absorbance coefficient occurs at  $2.05 \text{ mm}^{-1}$ .

The transparent drain absorbs a small amount of radiation for each tested wavelengths. The highest absorption coefficient ( $0.11 \text{ mm}^{-1}$ ) occurred at the wavelength representing UV radiation (353.5 nm).

#### Surface topography studies

The average values of the  $S_a$  parameter are presented depending on the type of drain and the side of the test (FIG. 14). Analysis of the roughness parameter  $S_a$  indicates greater roughness of the transparent drain compared to the amber drain. The inner side of the two types of drains is characterized by a lower roughness, which is a more desirable situation due to the kinematics of drug flow in the drain.

The obtained surface topography results should be treated with uncertainty due to the way the samples were prepared. Placing the drains between microscope slides and heating them to high temperatures can introduce changes in their surface.

#### Surface wettability studies

Both amber and transparent drains show hydrophobic characteristics (FIG. 15).

Wettability tests of drains showed their variation depending on the type of drain and surface (internal, external). A lower value of the wetting angle was observed for the transparent drain, indicating its greater wettability compared to the amber drain.

Based on the results obtained, it is not possible to clearly say which side of the drain (external/internal) has greater wettability. For the transparent drain, we observed a larger wetting angle for the outer side. For the amber drain, on the other hand, we observed the opposite situation - a smaller wetting angle for the outer side, but the wide range of standard deviation should be kept under consideration.

The results of wetting angle measurements should be treated with some uncertainty. The preparation of the samples required deformation of the drains at high temperature, which may affect changes in the surface of the material and thus the obtained results.

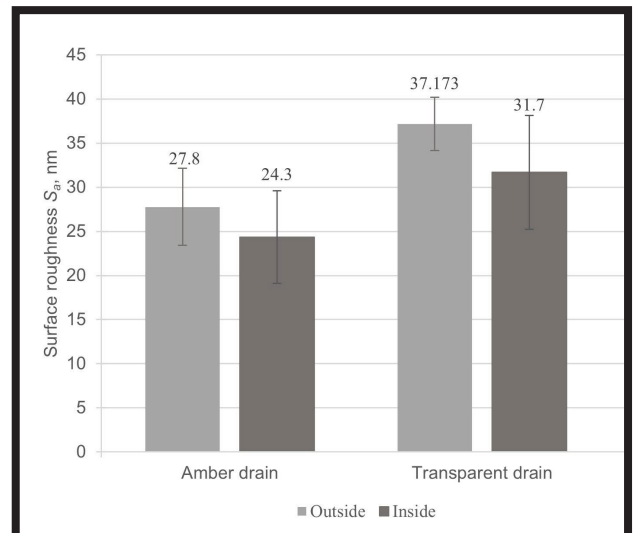


**FIG. 14. The average values of the surface roughness ( $S_a$ ) depending on the type of the drain and side of the tested surface.**

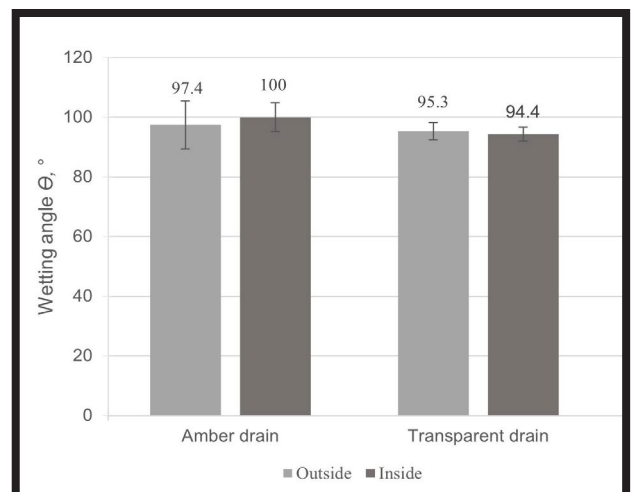


**FIG. 15. The average value of the wetting angle to the type of drain and side of the test.**

## Conclusions

Both transparent and amber drains were made of PVC material. TOTM plasticizer was added to the transparent and amber drains, and octadecanoic acid was added only to the amber drain. According to manufacturer's information, the amber color of the drains was obtained by adding bis(2-ethylhexyl) phosphite. Its FTIR spectrum overlaps with the PVC spectrum, which can make it difficult to identify.

Transparent and amber drains have different optical properties. Transparent drain is characterized by high transmission in the entire UV-VIS range, which can cause negative radiation effects on photosensitive drugs. Amber drain is characterized by lower transmittance compared to transparent drains. The transmittance of the amber drain in the 400-500 nm range is close to zero and for higher wavelengths, it successively increases to about 80%.

Improved protection of the photosensitive drug from damaging radiation can be achieved by increasing the wall thickness of the drains. Doubling the thickness of the amber drain wall will result in a four-fold reduction of radiation transmittance in the entire UV-VIS range, which means almost complete elimination of harmful radiation. It is also possible to increase the thickness of the transparent drain, but this would be an impractical solution, so it is worth considering adding bis(2-ethylhexyl) phosphite (a component of the amber drain) in an amount that guarantees the protection of photosensitive drugs.

Both the amber and transparent drains show hydrophobic characteristics. It is impossible to clearly say which of the tested sides (outer/internal) of the drains shows a lower wettability, but the inner side is characterized by a lower roughness, which is significantly conducive to drug flow.

## Acknowledgements

*I would like to thank Zarys Company for providing information on the composition of the studied material and Dr. Joanna Jaworska for her support in analyzing the FTIR-ATR spectrophotometric results.*

### ORCID ID

K. Szafarczyk:  <https://orcid.org/0009-0005-4711-6259>  
 J. Szewczenko:  <https://orcid.org/0000-0001-9718-8617>  
 E. Maciak:  <https://orcid.org/0000-0002-0620-4931>  
 P. Kałużński:  <https://orcid.org/0000-0001-6559-4944>  
 K. Goldsztajn:  <https://orcid.org/0000-0003-2545-9339>

## References

- [1] Lee P.: Infusion pump development and implications for nurses. *British Journal of Nursing* 24(19) (2015) 30-37.
- [2] Sánchez-Quiles I., Nájera-Pérez M.D., Espuny-Miró A., Titos-Arcos J.C.: Review of the Stability of Photosensitive Medications. *Farmacia Hospitalaria* 35(4) (2011) 204-215.
- [3] Website: <https://rejestrmedyczne.ezdrowie.gov.pl/rpl/search/public> (access: 02.11.2022).
- [4] Website: <https://zarys.pl/katalogi/> (access: 18.12.2022).
- [5] Oblój-Muzaj M., Świerż-Motyś B., Szablowska B.: Polichlorek winylu. Wydawnictwo Naukowo-Techniczne, Warszawa 1997.
- [6] Dobrzański L.A.: Podstawy nauki o materiałach i metaloznawstwo – Materiały inżynierskie z podstawami projektowania materiałowego. Wydawnictwo Naukowo-Techniczne, Warszawa 2002.
- [7] Rabek J.F.: Współczesna wiedza o polimerach – Budowa strukturalna polimerów i metody badawcze. Wydawnictwo Naukowe PWN SA, Warszawa 2017.
- [8] Nowicka-Jankowska T.: Spektrofotometria UV/VIS w analizie chemicznej. Państwowe Wydawnictwo Naukowe, Warszawa 1988.
- [9] Lai H., Wang Z., Wu P., Chaudhary B.I., Sengupta S.S., Cogen J.M., Li B.: Structure and Diffusion Behavior of Trioctyl Trimellitate (TOTM) in PVC Film Studied by ATR-IR Spectroscopy. *Industrial & Engineering Chemistry Research* 51(27) (2012) 9365-9375.
- [10] Website: <https://webbook.nist.gov/cgi/cbook.cgi?ID=C3319311&Units=SI&Mask=80#IR-Spec> (access: 10.01.2023).
- [11] Website: <https://webbook.nist.gov/cgi/cbook.cgi?ID=C57114&Units=SI&Type=IR-SPEC&Index=3#IR-SPEC> (access: 10.01.2023).
- [12] Website: <https://spectrabase.com/spectrum/DfQFrsth30> (access: 10.01.2023).
- [13] Website: <https://spectrabase.com/spectrum/ENsh126hyM1> (access: 10.01.2023).

# COMPOSITES BASED ON POLYVINYL ALCOHOL, CHITOSAN, AND CURCUMIN FOR WOUND HEALING APPLICATIONS

MUHAMMAD TAHIR<sup>1\*</sup> , SILVIA VICINI<sup>2</sup> ,  
ALINA SIONKOWSKA<sup>1</sup> 

<sup>1</sup> DEPARTMENT OF BIOMATERIALS AND COSMETIC CHEMISTRY, FACULTY OF CHEMISTRY, NICOLAUS COPERNICUS UNIVERSITY IN TORUŃ, GAGARINA 7, 87-100 TORUŃ, POLAND

<sup>2</sup> DEPARTMENT OF CHEMISTRY AND INDUSTRIAL CHEMISTRY, UNIVERSITY OF GENOVA, VIA DODECANESO 31, GENOA 16146, ITALY

\*E-MAIL: 503438@DOKTORANT.UMK.PL

## Abstract

*Natural polymers, like chitosan, collagen, and alginate, offer promising solutions for wound healing. Derived from natural sources, they exhibit biocompatibility and bioactivity, promoting tissue regeneration. These polymers can form scaffolds or dressings that accelerate wound closure while reducing infection risks. Their inherent properties make them promising options in the quest for effective wound care materials.*

*In this work, composites based on polyvinyl alcohol (PVA), chitosan (Chi), and curcumin (Cur) were prepared. PVA, a synthetic water-soluble polymer, finds extensive use in biomedical and wound-healing applications. It is approved by the U.S. FDA for cosmetic, medical, and wound healing products. Chi, a polysaccharide, is widely used in biomedicine and possesses antibacterial properties. Both PVA and chitosan are biocompatible and exhibit good film-forming characteristics. Curcumin (Cur) with antibacterial and antioxidant properties is being explored for regenerative medicine. PVA, chitosan, and curcumin were blended. The structure was studied by FTIR, microscopic observations were done with optical and scanning electron microscopes, and the mechanical properties were assessed. FTIR revealed component interactions, while microscopy showed a flat film surface. The polymeric blend (PVA/Chi/Cur) had a Young's modulus of 1.49 GPa, tensile strength of 47.69 MPa, stress value of 8.39 N, and 35.34% elongation at break. These properties make the blend suitable for consideration in wound healing applications.*

**Keywords:** polyvinyl alcohol, chitosan, curcumin, polymer blends, wound healing

## Introduction

Poly(vinyl alcohol) (PVA) is a semi-crystalline and water-soluble polymer [1]. PVA exhibits limited solubility in ethanol and is insoluble in other organic solvents [2]. The preparation of poly(vinyl alcohol) is achieved through the hydrolysis of poly(vinyl acetate) and can be easily degraded by biological microorganisms [3]. PVA is considered ideal for wound dressings due to its non-toxicity, biodegradability, and low cost [4]. The properties of poly(vinyl alcohol) are highly dependent on the acetyl group content in the initial polymer [5]. The applications of poly(vinyl alcohol) are determined by its degree of hydrolysis [6]. Tavakoli et al. utilized poly(vinyl alcohol) with a degree of hydrolysis of 99.9% for wound healing applications [7]. Murphy et al. employed poly(vinyl alcohol) with degrees of hydrolysis of 88% and 98%. It has been suggested and recommended to use poly(vinyl alcohol) with a higher degree of hydrolysis for wound healing applications [8]. PVA wound dressings are non-adhesive, making them suitable for easy dressing changes without causing new wound injury [9].

Chitosan is a polysaccharide of marine origin [10] and is often described as a natural cationic polymer with a positive charge [11,12]. Chitosan is derived from chitin, a fundamental component of crustacean shells, through chemical modification [13]. Chitin is insoluble in water due to extensive hydrogen bonding [14], while chitosan can be dissolved in weaker acids, like acetic acid, to form membranes and fibers [15]. Chitosan contains amine functional groups, and these groups can be chemically modified, making Chi very useful for biomedical applications [16]. Chitosan is widely applied in the pharmaceutical and biomedical fields as it has interesting properties [17], such as high biocompatibility, anticancer properties, blood clotting facilitation, and coagulation effects [18].

Wound healing involves various phases, such as inflammation, proliferation, and tissue remodeling, making it a complex process requiring specialized treatments [19]. A good wound dressing should facilitate gaseous exchange, maintain wound surface moisture, and be able to remove extra wound fluid or exudates [20]. The obvious reason for using chitosan in wound healing is its ability to enhance healing and skin restoration [21,22], and it has been reported as highly applicable in regenerative medicine [23]. Chitosan also aids in blood coagulation and adheres to red blood cells due to its hemostatic nature [24,25].

The use of chitosan as a standalone wound healing material may lead to loss of strength after absorbing the wound exudates, resulting in decomposition. To prevent disintegration, it is often combined with other compounds, such as synthetic polymers like poly(vinyl alcohol) [26-28]. A significant limitation of using chitosan alone in wound dressings is its insolubility in water [29]. Chitosan is frequently blended with PVA to enhance the antibacterial properties of the resulting hydrogel [30].

[Engineering of Biomaterials 167 (2022) 10-16]

doi:10.34821/eng.biomat.167.2022.10-16

Submitted: 2023-04-03, Accepted: 2023-04-26, Published: 2023-04-30



Copyright © 2022 by the authors. Some rights reserved.  
Except otherwise noted, this work is licensed under  
<https://creativecommons.org/licenses/by/4.0>

Curcumin, a yellow-colored polyphenol, is naturally found in the rhizome of *Curcuma longa* [31]. It is also known as difluoromethane [32,33]. Curcumin is hydrophobic and can be dissolved in ethanol, acetone, and dimethyl sulphoxide [34]. It has antioxidant, anticarcinogenic, anti-inflammatory, and anticoagulation properties. Curcumin shows a promising role in wound healing [35,36], primarily by participating in tissue remodeling, collagen deposition, and tissue formation [37]. Fianza et al. noted its effectiveness in the inflammation stage of wound healing due to its role in reducing reactive oxygen species [38]. Curcumin is also capable of scavenging free radicals [39], as it can share electrons or hydrogen atoms from its phenolic sites. Additionally, it acts as a lipophilic compound [40]. Li et al. utilized chitosan nanoparticles with curcumin, improving the wound healing process in diabetic rat models [41]. Alven et al. reported that wound dressings containing curcumin improved mechanical properties and enhanced wound healing [42]. Akbik et al. emphasized that curcumin plays a vital role in all stages of the wound healing process [43]. Rezaei et al. suggested that blending curcumin with polymeric solutions is the best approach to control its release in biomedical applications [44]. The use of curcumin is limited due to its poor water solubility and photosensitivity [34], with a substantial portion of orally administered curcumin passing undigested through the gastrointestinal system [45,46].

In this study, polymeric blends of poly(vinyl alcohol), chitosan, and curcumin were prepared. We analyzed the mechanical properties of the resulting polymeric blend and conducted microscopic analysis of the polymeric film. Fourier Transform Infrared (FTIR) spectra were recorded to investigate functional groups. Chitosan and poly(vinyl alcohol) were incorporated into the film, indicating potential wound healing properties. Furthermore, curcumin, with its antioxidant properties, may improve wound healing. Therefore, combining wound healing materials such as poly(vinyl alcohol) and chitosan with curcumin may offer new materials for biomedical applications with enhanced properties.

## Materials and Methods

Poly(vinyl alcohol) (363065, CAS:9002-89-2, MW: 146,000-186,000), and chitosan (448869, CAS:9012-76-4, MW: 50,000-190,000) were obtained from Sigma-Aldrich, Darmstadt, Germany. Curcumin (GP8291, CAS: 458-37-7, MW: 368.39) was received from Glentham Life Sciences, Corsham, United Kingdom. Ethanol (Cat. 32294, CAS: 64-17-5, MW: 46.07, 96%) was provided by Honeywell, Riedel-de Haen, Seelze, Germany. Acetic acid (CAS:64-19-7, MW: 60.05, 99.9%) from STANLAB, Lublin, Poland, was used.

## Sample preparation

At the beginning, the following solutions were prepared: 5% polyvinyl alcohol (PVA) in water, 2% chitosan (Chi) in acetic acid, and 5 mg curcumin (Cur) in 5 mL of ethanol. PVA/Chi polymeric blend was formulated in a 50:50 proportion, next 2% of dissolved curcumin was added to the polymeric blend. Polymeric films of PVA, Chi, and polymeric blend (PVA/Chi/Cur) were prepared by solvent casting.

## Microscopic analysis

Microscopic analysis of the surface of the polymeric films was carried out using a Motic microscope (SMZ-171, China) with 0.75 resolution and with a scanning electron microscope (SEM; LEO, Electron Microscopy Limited, Cambridge, UK).

## Fourier Transform Infrared Spectroscopy (FTIR)

Fourier Transform Infrared (FTIR) spectra of the polymeric films and curcumin powder were analyzed using Nicolet iS10 furnished with an ATR device (Thermo Fisher Scientific, Waltham, MA, USA). The spectrum was recorded in the 400-4000  $\text{cm}^{-1}$  range with a resolution of 4  $\text{cm}^{-1}$  following 64 scans. Omnic 2009 software was used for spectra processing.

## Mechanical properties testing

Mechanical properties of the PVA, Chi, PVA/Cur, PVA/Chi/Cur films were analyzed using Zwick and Roell 0.5 testing machine combined with testXpert II 2017 software. Seven samples of each type were investigated. The initial test parameters were: 0.1 MPa preload, 5 mm/min preload speed, and 50 mm/min test speed.

## Statistical Analysis

ANOVA test was used for statistical analysis. The variance was checked by following the standard deviation results.

## Results and Discussions

Microscopic analysis of polymeric films is presented in FIG. 1. FIG. 1a illustrates the microscopic image of PVA and clearly shows a smooth surface. In FIG. 1b PVA and Cur have been mixed homogeneously. In this figure, the curcumin effect can be seen in the polymeric blend, as it changed the color of the polymeric blend to a pale-yellow color. FIG. 1c represents the polymeric blend (PVA/Chi/Cur). It can be noticed that PVA, Chi, and Cur are compatible in the polymeric blend and are homogeneously mixed. This uniformity or homogeneity is achieved due to the stirring of polymeric solutions for 24 h and the interaction between PVA and chitosan via hydrogen bonds.

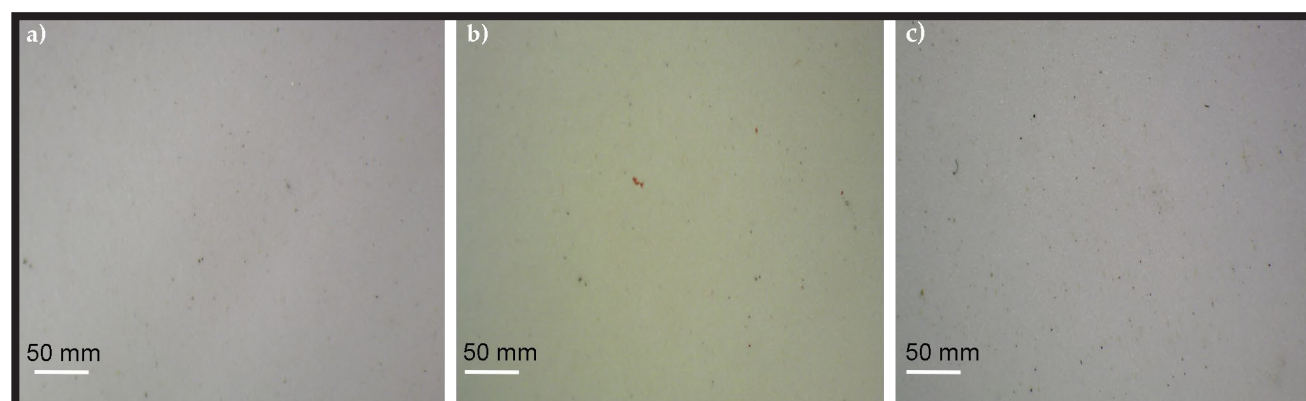


FIG. 1. Microscopic images of polymeric films: a) PVA, b) PVA/Cur, c) PVA/Chi/Cur.

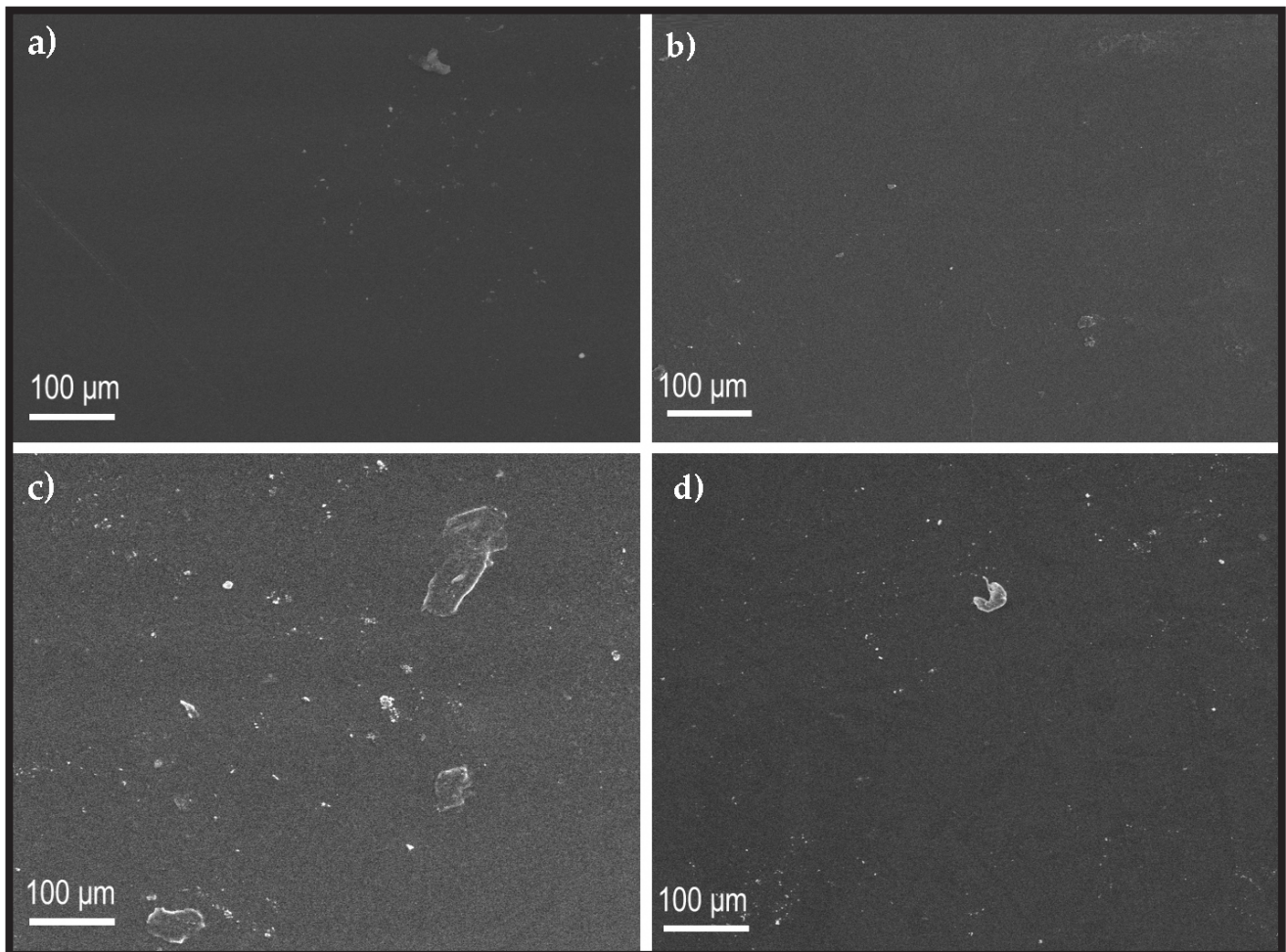


FIG. 2. SEM images: a) Chi, b) PVA, c) PVA/Cur, d) PVA/Chi/Cur.

SEM images are presented in FIG. 2 to view the morphology of the polymeric films of individual polymers and their polymeric blends. FIG. 2a presents SEM image of chitosan (Chi), which can be seen as a flat and smooth surface; a similar analysis has been reported in the literature [47,48]. FIG. 2b shows SEM image of the polyvinyl alcohol (PVA) films, and it demonstrates the uniformity of the surface. It also shows the presence of few flakes, which can be caused due to the semicrystalline nature of poly(vinyl alcohol). The uniformity of the PVA surface has been described by Mahesh et al. [49]. FIG. 2c presents the SEM image of PVA/Cur, showing the presence of curcumin throughout the surface in the form of agglomerates. FIG. 2d shows SEM image of the polymeric blend (PVA/Chi/Cur), and it displays a smooth and uniform surface with agglomerates due to the presence of curcumin. The smooth and uniform surface of PVA/Chi has been described by Costa-Júnior et al. [50].

Fourier Transform Infrared (FTIR) spectroscopy results are depicted in FIG. 3. It presents a comparative stack analysis of all recorded spectra. The FTIR spectrum of chitosan (Chi) shows an intense band at  $3265\text{ cm}^{-1}$  resulting from the overlap of the O-H and N-H bonds as mentioned by Kulig et al. [51]. The higher peak at  $2921\text{ cm}^{-1}$  and the lower-intensity peak at  $2872\text{ cm}^{-1}$  are due to the C-H stretching [52]. The peak at  $1633\text{ cm}^{-1}$  is caused due to the -CONHR group and the peak at  $1540\text{ cm}^{-1}$  is due to the amine group [53]. The reason for the peaks that appeared at  $1404\text{ cm}^{-1}$ , and  $1377\text{ cm}^{-1}$  is the  $\text{CH}_3$  symmetrical deformation. The intense peak at  $1023\text{ cm}^{-1}$  describes the C-O stretching [54].

The main peaks observed in the FTIR spectrum of polyvinyl alcohol (PVA) are related to hydroxyl and acetate groups because polyvinyl alcohol is prepared by hydrolysis of poly(vinyl acetate). The largest peak was observed at  $3259\text{ cm}^{-1}$  ( $\nu$  O-H). The peak observed with the O-H functional group is due to intermolecular and intramolecular hydrogen bonding. The peaks observed at  $2905\text{ cm}^{-1}$  ( $\nu$  C-H alkyl group) [55,56], the peaks noticed at  $1651\text{ cm}^{-1}$ , and  $1141\text{ cm}^{-1}$  are due to the stretches of the carboxyl group [57]. The strong peak is presented at  $1563\text{ cm}^{-1}$ . Deshkulkarni et al. have mentioned that this peak is due to the benzenoid ring [58]. The sharp band appeared at  $1084\text{ cm}^{-1}$  and is due to the C-O stretching of the C-O-H group. Stretching vibrations have been observed at  $916\text{ cm}^{-1}$  and  $832\text{ cm}^{-1}$  due to the C-H group [59].

FTIR spectra of curcumin (Cur) have demonstrated the characteristic bands at  $2944$ ,  $2846$  and  $1428\text{ cm}^{-1}$ . These characteristic bands are due to the C-H stretching and because of the deformation of the methyl groups - similar results were presented in the literature by Abadeh [60]. Curcumin (Cur) has also shown a medium intensity peak at  $3510\text{ cm}^{-1}$  ( $\nu$  O-H phenol),  $1628\text{ cm}^{-1}$  ( $\nu$  C=O ketonic), and  $1277\text{ cm}^{-1}$  ( $\nu$  C-O phenol). Strong intensity peaks have been shown at  $1602\text{ cm}^{-1}$  ( $\nu$  C=O ketonic) and  $1509\text{ cm}^{-1}$  ( $\nu$  C=C aliphatic) [61].

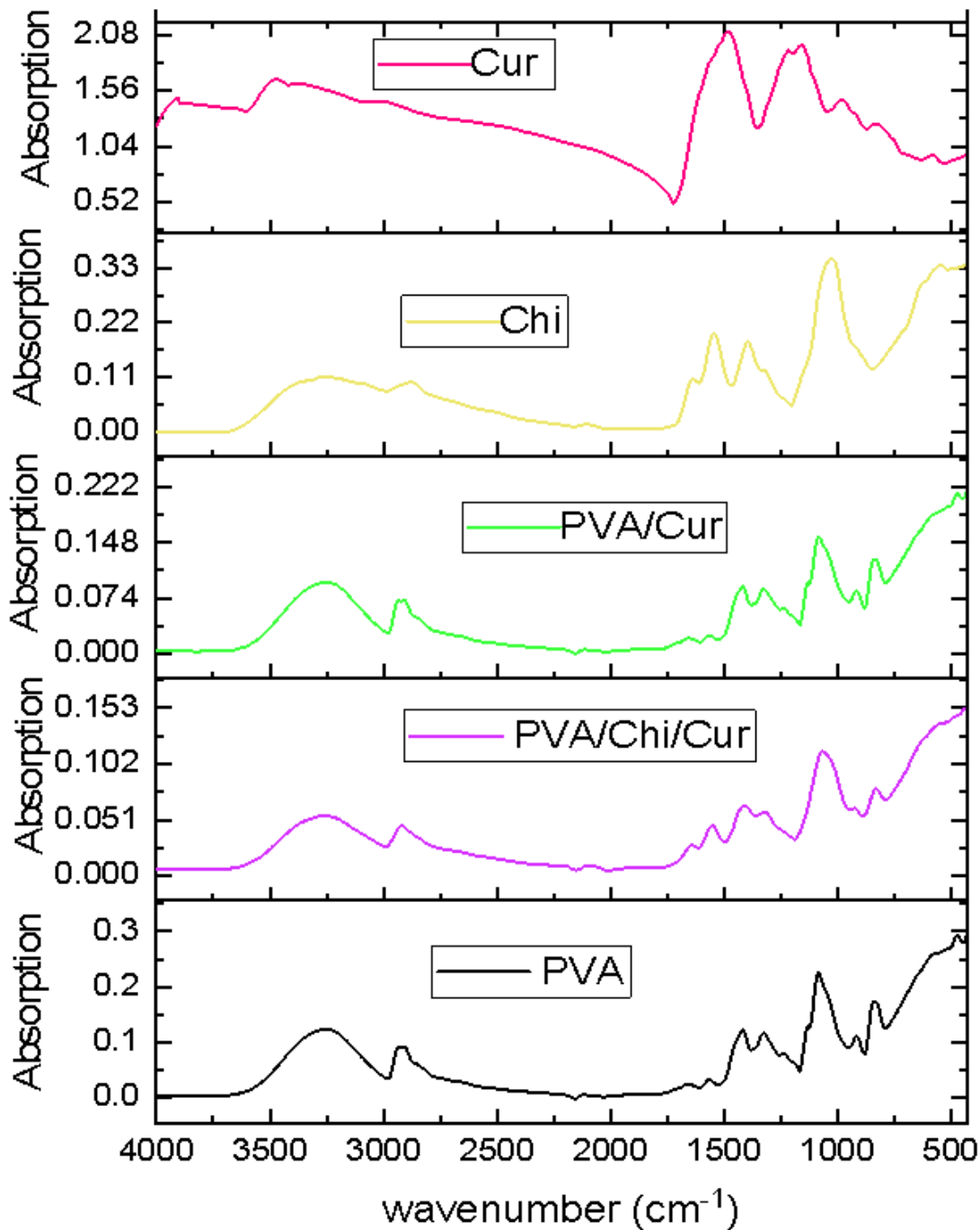


FIG. 3. Comparative stack spectrum of polymeric films and curcumin powder.

The FTIR spectrum of PVA/Cur was analyzed, and it presented the absorption band at  $3260\text{ cm}^{-1}$ , resulting from the OH groups and intermolecular hydrogen bonding between them. A band at  $1560\text{ cm}^{-1}$  is caused by the carboxylate group, or due to the inter-molecularly bonded water. The peak at  $1416\text{ cm}^{-1}$  comes from the polyvinyl alcoholic groups. The peak at  $1375\text{ cm}^{-1}$  is resulted due to the addition of curcumin (Cur). The addition of curcumin to the polymeric solution of polyvinyl alcohol modified the FTIR peaks.

The FTIR spectrum of the polymeric blend of PVA/Chi/Cur presents the absorption band at  $3254\text{ cm}^{-1}$  and it is caused by the intermolecular hydrogen bonding with the presence of O-H functional group. The peak at  $2938\text{ cm}^{-1}$  is due to the presence of the alkyl group. A band that appeared at  $1555\text{ cm}^{-1}$  is due to the amine group of chitosan. The peak at  $1378\text{ cm}^{-1}$  is due to the presence of curcumin in the polymeric blend. The addition of chitosan modified the position of the peaks of the polymeric blend of the PVA/Cur which suggests the interactions between polymers via hydrogen bonds. FTIR spectra have also confirmed morphological studies of the polymeric films in the form of the functional groups presence.

The results of the mechanical properties of the polymeric films are presented in TABLE 1. The results in the table are indicated as the average value with the standard deviation value. The highest value of Young's modulus was observed in the case of chitosan films (Chi), and the lowest Young's modulus was obtained in the case of poly(vinyl alcohol) films (PVA). The tensile strength was the highest for chitosan (Chi), and the tensile strength was the lowest for the polymeric blend (PVA/Chi/Cur). The highest value of breaking force or stress was recorded for PVA, and it was the lowest in the polymeric blend (PVA/Chi/Cur). Elongation percentage presented the highest value for polyvinyl alcohol (PVA), whereas the lowest value was found for the chitosan film (Chi).

The results of mechanical properties are presented in the form of bar graphs in FIGs. 4, 5, 6, and 7. The bar graphs show the mechanical properties average value with the error bars. Error values have been calculated following the standard deviation values, and the standard deviation has been calculated following the variance. These values were obtained with the help of the ANOVA test. The mechanical properties of the blend prepared in this research are sufficient for applications as wound dressing.

**TABLE 1. Mechanical properties of polymers.**

Sr. No.	Polymers	Young's Modulus [GPa]	Tensile Strength [MPa]	Stress [N]	Elongation [%]
1	PVA	0.99 ± 0.22	49.04 ± 1.30	13.20 ± 2.65	180.09 ± 27.09
2	Chi	3.11 ± 0.69	69.43 ± 3.69	10.77 ± 1.76	7.83 ± 1.23
3	PVA/Cur	1.00 ± 0.24	50.39 ± 1.63	13.09 ± 2.37	145.91 ± 22.67
4	PVA/Chi/Cur	1.49 ± 0.36	47.69 ± 3.85	8.39 ± 4.29	35.34 ± 19.28

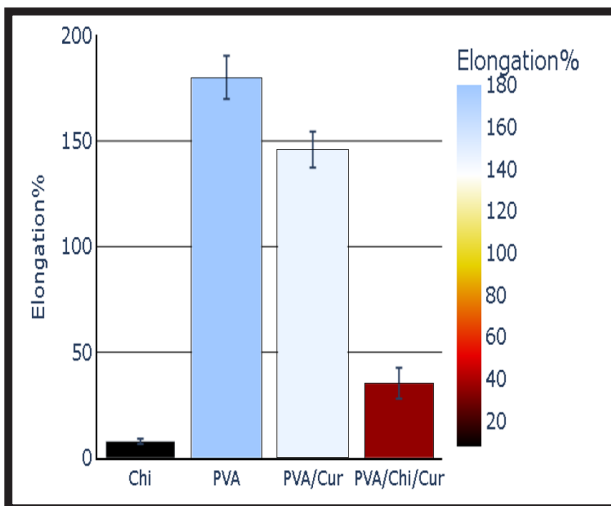


**FIG. 4. Elongation at break of polymer films.**

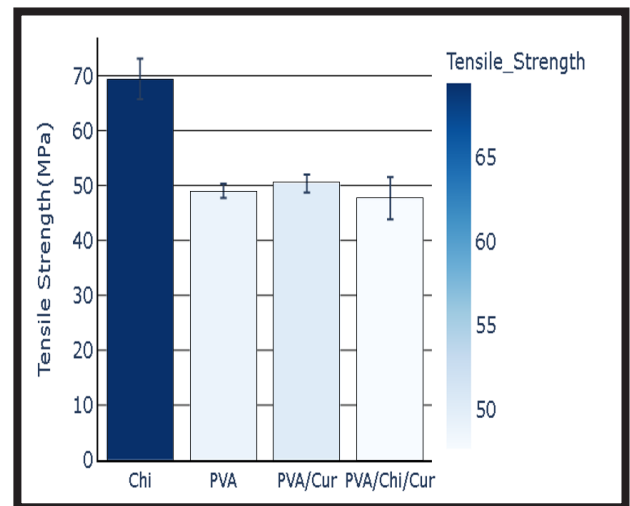


**FIG. 6. Tensile strength of polymer films.**

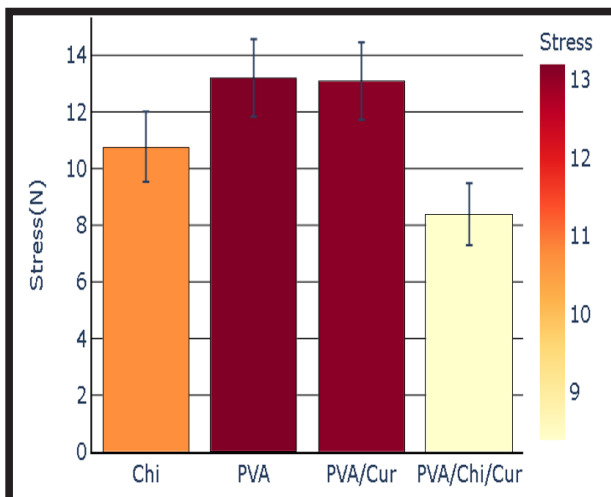


**FIG. 5. Stress of polymer films.**

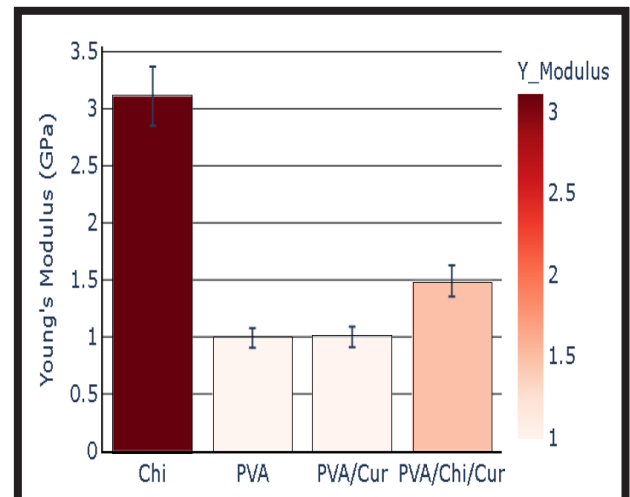


**FIG. 7. Young's Modulus of polymer films.**

## Conclusions

A polymer composite based on the blend of PVA and chitosan with curcumin has been successfully obtained. The presence of components in the composite was confirmed by FTIR spectroscopy. The mechanical properties of the composite were different than those of the single components. The elasticity and elongation percentage of the chitosan film was observed with a rather small value. The PVA polymeric blend containing chitosan showed decreased ductility and elongation percentage. The elasticity of the polymeric blend containing polyvinyl alcohol, curcumin, and chitosan was found to be higher than those for the chitosan film. The composite obtained in this study may help to maintain a moist environment for the wound and increase the protection against microbial attack and to prevent the wound from open exposure to oxygen.

## Acknowledgments

*This research has not received external funding.*

### ORCID iD

M. Tahir: <https://orcid.org/0000-0001-8436-1126>  
 S. Vicini: <https://orcid.org/0000-0001-9369-1522>  
 A. Sionkowska: <https://orcid.org/0000-0002-1551-2725>

## References

- [1] Gobi R., Babu R.S.: In-vitro study on chitosan/PVA incorporated with nickel oxide nanoparticles for wound healing application. *Mater Today Commun.* 34 (2023) 105154. <https://doi.org/10.1016/J.MTCOMM.2022.105154>
- [2] Marin E., Rojas J., Ciro Y.: A review of polyvinyl alcohol derivatives: promising materials for pharmaceutical & biomedical applications. *Afr J Pharm Pharmacol.* 8, (2014) 674-684. <https://doi.org/10.5897/AJPP2013.3906>
- [3] Razzak M.T., Darwis D., Zainuddin S.: Irradiation of polyvinyl alcohol and polyvinyl pyrrolidone blended hydrogel for wound dressing. *Radiation Physics and Chemistry.* 62 (2001) 107-113. [https://doi.org/10.1016/S0969-806X\(01\)00427-3](https://doi.org/10.1016/S0969-806X(01)00427-3)
- [4] Jin S.G.: Production and Application of Biomaterials Based on Polyvinyl alcohol (PVA) as Wound Dressing. *Chem Asian J.* 17 (2022) e202200595. <https://doi.org/10.1002/ASIA.202200595>
- [5] Hassan C.M., Peppas N.A.: Structure and applications of poly(vinyl alcohol) hydrogels produced by conventional crosslinking or by freezing/thawing methods. *Advances in Polymer Science.* 153 (2000) 37-65.
- [6] Haweel C.K., Ammar S.H.: Preparation of Polyvinyl Alcohol from Local Raw Material. *Iraqi Journal of Chemical and Petroleum Engineering* 9 (2008) 15-21.
- [7] Tavakoli J., Mirzaei S., Tang Y.: Cost-Effective Double-Layer Hydrogel Composites for Wound Dressing Applications. *Polymers* 10 (2018) 305. <https://doi.org/10.3390/POLYM10030305>
- [8] Murphy D.J., Sankalia M.G., Loughlin R.G., Donnelly R.F., Jenkins M.G., Mccarron P.A.: Physical characterisation and component release of poly(vinyl alcohol)-tetrahydroxyborate hydrogels and their applicability as potential topical drug delivery systems. *Int J Pharm.* 423 (2012) 326-334. <https://doi.org/10.1016/J.IJPHARM.2011.11.018>
- [9] Gao T., Jiang M., Liu X., You G., Wang W., Sun Z., Ma A., Chen J.: Patterned Polyvinyl Alcohol Hydrogel Dressings with Stem Cells Seeded for Wound Healing. *Polymers* 11 (2019) 171. <https://doi.org/10.3390/POLYM11010171>
- [10] Petroni S., Tagliaro I., Antonini C., D'Arienzo M., Orsini S.F., Mano J.F., Brancato V., Borges J., Cipolla L.: Chitosan-Based Biomaterials: Insights into Chemistry, Properties, Devices, and Their Biomedical Applications. *Marine Drugs* 21 (2023) 147. <https://doi.org/10.3390/MD21030147>
- [11] Choi C., Nam J.P., Nah J.W.: Application of chitosan and chitosan derivatives as biomaterials. *Journal of Industrial and Engineering Chemistry.* 33 (2016) 1-10. <https://doi.org/10.1016/J.JIEC.2015.10.028>
- [12] Bai Q., Gao Q., Hu F., Zheng C., Chen W., Sun N., Liu J., Zhang Y., Wu X., Lu T.: Chitosan and hyaluronic-based hydrogels could promote the infected wound healing. *Int J Biol Macromol.* 232 (2023) 123271. <https://doi.org/10.1016/J.IJBIOMAC.2023.123271>
- [13] Rinaudo M.: Chitin and chitosan: Properties and applications. *Prog Polym Sci.* 31 (2006) 603-632.
- [14] Gocho H., Shimizu H., Tanioka A., Chou T.J., Nakajima T.: Effect of polymer chain end on sorption isotherm of water by chitosan. *Carbohydr Polym.* 41 (2000) 87-90. [https://doi.org/10.1016/S0144-8617\(99\)00113-7](https://doi.org/10.1016/S0144-8617(99)00113-7)
- [15] Azad A.K., Sersintham N., Chandkrachang S., Stevens W.F.: Chitosan membrane as a wound-healing dressing: Characterization and clinical application. *J Biomed Mater Res B Appl Biomater.* 69B (2004) 216-222. <https://doi.org/10.1002/JBM.B.30000>
- [16] Campos E.V.R., Oliveira J.L., Fraceto L.F.: Poly(ethylene glycol) and cyclodextrin-grafted chitosan: From methodologies to preparation and potential biotechnological applications. *Front Chem.* 5 (2017) 290384. <https://doi.org/10.3389/FCHEM.2017.00093/BIBTEX>
- [17] Berger J., Reist M., Mayer J.M., Felt O., Peppas N.A., Gurny R.: Structure and interactions in covalently and ionically crosslinked chitosan hydrogels for biomedical applications. *European Journal of Pharmaceutics and Biopharmaceutics.* 57 (2004) 19-34. [https://doi.org/10.1016/S0939-6411\(03\)00161-9](https://doi.org/10.1016/S0939-6411(03)00161-9)
- [18] Jayabal P., Kannan Sampathkumar V., Vinothkumar A., Mathapati S., Pannerselvam B., Achiraman S., Venkatasubbu G.D.: Fabrication of a Chitosan-Based Wound Dressing Patch for Enhanced Antimicrobial, Hemostatic, and Wound Healing Application. *ACS Appl Bio Mater.* 6 (2023) 615-627. <https://doi.org/10.1021/ACSABM.2C00903>
- [19] Chopra H., Bibi S., Kumar S., Khan M.S., Kumar P., Singh I.: Preparation and Evaluation of Chitosan/PVA Based Hydrogel Films Loaded with Honey for Wound Healing Application. *Gels* 8 (2022) 111. <https://doi.org/10.3390/GELS8020111>
- [20] Jayakumar R., Prabakaran M., Sudheesh Kumar P.T., Nair S.V., Tamura H.: Biomaterials based on chitin and chitosan in wound dressing applications. *Biotechnol Adv.* 29 (2011) 322-337. <https://doi.org/10.1016/J.BIOTECHADV.2011.01.005>
- [21] Değim Z., Çelebi N., Sayan H., Babül A., Erdoğan D., Take G.: An investigation on skin wound healing in mice with a taurine-chitosan gel formulation. *Amino Acids.* 22 (2002) 187-198. <https://doi.org/10.1007/S007260200007/METRICS>
- [22] Singh R., Shitiz K., Singh A.: Chitin and chitosan: biopolymers for wound management. *Int Wound J.* 14 (2017) 1276-1289. <https://doi.org/10.1111/IWJ.12797>
- [23] Amor I.B., Emran T.B., Hemmami H., Zeghoud S., Laouini S.E.: Nanomaterials based on chitosan for skin regeneration: an update. *Int J Surg.* 109 (2023) 594-596. <https://doi.org/10.1097/JS9.000000000000181>
- [24] Paul W., Sharma C.P.: Chitosan and alginate wound dressings: a short review. *Trends Biomater Artif Organs.* 18 (2004) 18-23.
- [25] Sakthiguru N., Sithique M.A.: Fabrication of bioinspired chitosan/gelatin/allantoin biocomposite film for wound dressing application. *Int J Biol Macromol.* 152 (2020) 873-883. <https://doi.org/10.1016/J.IJBIOMAC.2020.02.289>

- [26] Zhang H., Xu Y., Lei Y., Wen X., Liang J.: Tourmaline nanoparticles modifying hemostatic property of chitosan/polyvinyl alcohol hydrogels. *Mater Lett.* 324 (2022) 132718. <https://doi.org/10.1016/J.MATLET.2022.132718>
- [27] Kanimozhi K., Khaleel Basha S., Sugantha Kumari V.: Processing and characterization of chitosan/PVA and methylcellulose porous scaffolds for tissue engineering. *Materials Science and Engineering: C.* 61 (2016) 484-491. <https://doi.org/10.1016/J.MSEC.2015.12.084>
- [28] Aldakheel F.M., Mohsen D., El Sayed M.M., Alawam K.A., Binshaya A.K.S., Alduraywish S.A.: Silver Nanoparticles Loaded on Chitosan-g-PVA Hydrogel for the Wound-Healing Applications. *Molecules* 28 (2023) 3241. <https://doi.org/10.3390/MOLECULES28073241>
- [29] Moeini A., Pedram P., Makvandi P., Malinconico M., Gomez d'Ayala G.: Wound healing and antimicrobial effect of active secondary metabolites in chitosan-based wound dressings: A review. *Carbohydr Polym.* 233 (2020) 115839. <https://doi.org/10.1016/J.CARPOL.2020.115839>
- [30] Zhang X.H., Yin Z., Guo Y., Huang H., Zhou J.Y., Wang L., Bai J.Y., Fan Z.: A facile and large-scale synthesis of a PVA/chitosan/collagen hydrogel for wound healing. *New Journal of Chemistry* 44 (2020) 20776-20784. <https://doi.org/10.1039/D0NJ04016A>
- [31] Zlotogorski A., Dayan A., Dayan D., Chaushu G., Salo T., Vered M.: Nutraceuticals as new treatment approaches for oral cancer - I: Curcumin. *Oral Oncol.* 49 (2013) 187-191. <https://doi.org/10.1016/J.ORALONCOLOGY.2012.09.015>
- [32] Aggarwal B.B., Kumar A., Bharti A.C.: Anticancer potential of curcumin: preclinical and clinical studies. *Anticancer Res.* 23, (2003) 363-398.
- [33] Pulido-Moran M., Moreno-Fernandez J., Ramirez-Tortosa C., Ramirez-Tortosa M.C.: Curcumin and Health. *Molecules* 21 (2016) 264. <https://doi.org/10.3390/MOLECULES21030264>
- [34] Sharma R.A., Gescher A.J., Steward W.P.: Curcumin: The story so far. *Eur J Cancer.* 41 (2005) 1955-1968. <https://doi.org/10.1016/J.EJCA.2005.05.009>
- [35] Devassy J.G., Nwachukwu I.D., Jones P.J.H.: Curcumin and cancer: barriers to obtaining a health claim. *Nutr Rev.* 73 (2015) 155-165. <https://doi.org/10.1093/NUTRIT/NUU064>
- [36] Panchatcharam, M., Miriyala, S., Gayathri, V.S., Suguna, L.: Curcumin improves wound healing by modulating collagen and decreasing reactive oxygen species. *Mol Cell Biochem.* 290, (2006) 87-96.
- [37] Joe B., Vijaykumar M., Lokesh B.R.: Biological Properties of Curcumin-Cellular and Molecular Mechanisms of Action. *Crit Rev Food Sci Nutr.* 44 (2010) 97-111. <https://doi.org/10.1080/10408690490424702>
- [38] Rezkita F., Wibawa K.G.P., Nugraha A.P.: Curcumin loaded chitosan nanoparticle for accelerating the post extraction wound healing in diabetes mellitus patient: A review. *Res J Pharm Technol.* 13 (2020) 1039-1042. <https://doi.org/10.5958/0974-360X.2020.00191.2>
- [39] Mohanty C., Sahoo S.K.: Curcumin and its topical formulations for wound healing applications. *Drug Discov Today.* 22 (2017) 1582-1592. <https://doi.org/10.1016/J.DRUDIS.2017.07.001>
- [40] Barzegar A., Moosavi-Movahedi A.A.: Intracellular ROS Protection Efficiency and Free Radical-Scavenging Activity of Curcumin. *PLoS One* 6 (2011) e26012. <https://doi.org/10.1371/JOURNAL.PONE.0026012>
- [41] Li F., Shi Y., Liang J., Zhao L.: Curcumin-loaded chitosan nanoparticles promote diabetic wound healing via attenuating inflammation in a diabetic rat model. *J Biomater Appl.* 34 (2019) 476-486. <https://doi.org/10.1177/0885328219860929>
- [42] Alven S., Nqoro X., Aderibigbe B.A.: Polymer-Based Materials Loaded with Curcumin for Wound Healing Applications. *Polymers* 12 (2020) 2286. <https://doi.org/10.3390/POLYM12102286>
- [43] Akbik D., Ghadiri M., Chrzanowski W., Rohanizadeh R.: Curcumin as a wound healing agent. *Life Sci.* 116 (2014) 1-7. <https://doi.org/10.1016/J.LFS.2014.08.016>
- [44] Rezaei M., Oryan S., Reza Nourani M., Mofid M., Mozafari M.: Curcumin nanoparticle-incorporated collagen/chitosan scaffolds for enhanced wound healing. *Bioinspired, Biomimetic and Nanobiomaterials* 7 (2018) 159-166. <https://doi.org/10.1680/JBIBN.17.00036>
- [45] Hassanizadeh S., Shojaei M., Bagherniya M., Orekhov A.N., Sahebkar A.: Effect of nano-curcumin on various diseases: A comprehensive review of clinical trials. *BioFactors* 49 (2023) 512-533. <https://doi.org/10.1002/BIOF.1932>
- [46] Nagpal M., Sood S.: Role of curcumin in systemic and oral health: An overview. *J Nat Sci Biol Med.* 4 (2013) 3. <https://doi.org/10.4103/0976-9668.107253>
- [47] Lewandowska K.: Surface studies of microcrystalline chitosan/poly(vinyl alcohol) mixtures. *Appl Surf Sci.* 263 (2012) 115-123. <https://doi.org/10.1016/J.APSUSC.2012.09.011>
- [48] Lewandowska K., Sionkowska A., Kaczmarek B., Furtos G.: Characterization of chitosan composites with various clays. *Int J Biol Macromol.* 65 (2014) 534-541. <https://doi.org/10.1016/J.IJBIOMAC.2014.01.069>
- [49] Mahesh B., Nanjundaswamy G.S., Kathyayani D., Gowda D.C., Siddaramaiah: Impact of Blend Proportion on the Miscibility and Thermal Characteristics of Synthetic Plastic-Derived Polypentapeptide with Commercially Available Polyvinyl Alcohol. *J Polym Environ.* 27 (2019) 2267-2280. <https://doi.org/10.1007/S10924-019-01511-1/FIGURES/12>
- [50] Costa-Júnior E.S., Barbosa-Stancioli E.F., Mansur A.A.P., Vasconcelos W.L., Mansur H.S.: Preparation and characterization of chitosan/poly(vinyl alcohol) chemically crosslinked blends for biomedical applications. *Carbohydr Polym.* 76 (2009) 472-481. <https://doi.org/10.1016/J.CARPOL.2008.11.015>
- [51] Kulig D., Zimoch-Korzycka A., Jarmoluk A., Marycz K.: Study on Alginate-Chitosan Complex Formed with Different Polymers Ratio. *Polymers* 8 (2016) 167. <https://doi.org/10.3390/POLYM8050167>
- [52] Mahmoud A.A., Osman O., Eid K., Al Ashkar E., Okasha A., Atta D., Eid M., Aziz Z.A., Fakhry A.: FTIR Spectroscopy of Natural Bio-Polymers Blends. *Middle East Journal of Applied Sciences* 4, (2014) 816-824.
- [53] Pokhrel S., Lach R., Grellmann W., Wutzler A., Lebek W., Godehardt R., Yadav P.N., Adhikari R.: Synthesis of chitosan from prawn shells and characterization of its structural and antimicrobial properties. *Nepal J Sci Technol.* 17 (2016) 5-9.
- [54] Wang T., Turhan M., Gunasekaran S.: Selected properties of pH-sensitive, biodegradable chitosan-poly (vinyl alcohol) hydrogel. *Polym Int.* 53 (2004) 911-918.
- [55] Mansur H.S., Sadahira C.M., Souza A.N., Mansur A.A.P.: FTIR spectroscopy characterization of poly (vinyl alcohol) hydrogel with different hydrolysis degree and chemically crosslinked with glutaraldehyde. *Materials Science and Engineering: C.* 28 (2008) 539-548. <https://doi.org/10.1016/J.MSEC.2007.10.088>
- [56] Mahesh B., Kathyayani D., Channe Gowda D., Mrutunjaya K.: Blends of synthetic plastic-derived polypeptide with Hydroxypropylmethylcellulose and polyvinyl alcohol: unraveling the specific interaction parameters, morphology and thermal stability of the polymers couple. *Journal of Polymer Research* 27 (2020) 1-15. <https://doi.org/10.1007/S10965-020-02191-5/FIGURES/12>
- [57] Latif I.A., Abdullah H.M., Saleem M.H.: Hydrogel permittivity, Swelling, Hydrogel, Chitosan, Pectin, Poly (vinyl alcohol), Conductive hydrogel. *American Journal of Polymer Science* 6 (2016) 50-57. <https://doi.org/10.5923/j.ajps.20160602.04>
- [58] Deshkulkarni B., Viannie L.R., Ganachari S.V., Banapurmath N.R., Shettar A.: Humidity sensing using polyaniline/polyvinyl alcohol nanocomposite blend. *IOP Conf Ser Mater Sci Eng.* 376 (2018) 1-8.
- [59] El-Nemr K.F., Mohamed H.R., Ali M.A., Fathy R.M., Dhmees A.S.: Polyvinyl alcohol/gelatin irradiated blends filled by lignin as green filler for antimicrobial packaging materials. *International Journal of Environmental Analytical Chemistry* 100 (2019) 1578-1602. <https://doi.org/10.1080/03067319.2019.1657108>
- [60] Ahali Abadeh Z., Saviano G., Ballirano P., Santonicola M.G.: Curcumin-loaded zeolite as anticancer drug carrier: effect of curcumin adsorption on zeolite structure. *Pure and Applied Chemistry* 92 (2020) 461-471. <https://doi.org/10.1515/pac-2018-1213>
- [61] Ismail E.H., Sabry D.Y., Mahdy H., Khalil M.M.H.: Synthesis and Characterization of some Ternary Metal Complexes of Curcumin with 1, 10-phenanthroline and their Anticancer Applications. *Journal of Scientific Research* 6 (2014) 509-519.

# CARTILAGE TISSUE EXAMINATION USING ATOMIC FORCE MICROSCOPY

JAROSŁAW PALUCH<sup>1</sup> , JAROSŁAW MARKOWSKI<sup>1\*</sup> , JAN PILCH<sup>1</sup> , WOJCIECH SMÓŁKA<sup>1</sup> , KRZYSZTOF PIOTR JASIK<sup>2</sup> , FILIP KILIAN<sup>3</sup> , WIRGINIA LIKUS<sup>4</sup> , GRZEGORZ BAJOR<sup>5</sup> , DARIUSZ CHROBAK<sup>6</sup> , KARSTEN GLOWKA<sup>6</sup> , OLIVIA STARCZEWSKA<sup>6\*\*</sup> 

<sup>1</sup> DEPARTMENT OF LARYNGOLOGY, FACULTY OF MEDICAL SCIENCES IN KATOWICE, MEDICAL UNIVERSITY OF SILESIA IN KATOWICE, FRANCUSKA 20/24, 40-055 KATOWICE, POLAND

<sup>2</sup> DEPARTMENT OF PATHOLOGY, FACULTY OF PHARMACEUTICAL SCIENCES IN SOSNOWIEC, MEDICAL UNIVERSITY OF SILESIA IN KATOWICE, OSTROGÓRSKA 30, 41-200 SOSNOWIEC, POLAND

<sup>3</sup> DEPARTMENT OF GENERAL, VASCULAR AND TRANSPLANT SURGERY, FACULTY OF MEDICAL SCIENCES IN KATOWICE, MEDICAL UNIVERSITY OF SILESIA IN KATOWICE, FRANCUSKA 20/24, 40-055 KATOWICE, POLAND

<sup>4</sup> DEPARTMENT OF ANATOMY, FACULTY OF HEALTH SCIENCES IN KATOWICE, MEDICAL UNIVERSITY OF SILESIA IN KATOWICE, MEDYKÓW 18, 40-752 KATOWICE, POLAND

<sup>5</sup> DEPARTMENT OF ANATOMY, FACULTY OF MEDICAL SCIENCES IN KATOWICE, MEDICAL UNIVERSITY OF SILESIA IN KATOWICE, MEDYKÓW 18, 40-752 KATOWICE, POLAND

<sup>6</sup> INSTITUTE OF MATERIALS ENGINEERING, UNIVERSITY OF SILESIA IN KATOWICE, 75 PUŁKU PIECHOTY 1A, 41-500 CHORZÓW, POLAND

\*E-MAIL: JMARKOW1@POCZTA.ONET.PL

\*\*E-MAIL: OLIVIA.STARCZEWSKA@US.EDU.PL

## Abstract

*Life sciences, a field closely intertwined with human biology and physiology, employ various research methods, including morphology studies and quantitative analysis through non-destructive techniques. Biological specimens often consist of three-phase structures, characterized by the presence of gas, liquid, and solid components. This becomes crucial when the chosen research methodology requires the removal of water from samples or their transfer to a cryostat.*

*In the current research, mechanical and topographical examination of cartilage was performed. The materials were generously provided by the Department of Anatomy at the Medical University of Silesia, thereby eliminating any concerns regarding their origin or ethical use for scientific purposes. Our research methodology involved the application of atomic force microscopy (AFM), which minimally disrupts the internal equilibrium among the aforementioned phases. Cartilage, recognized as a 'universal support material' in animals, proves to be highly amenable to AFM research, enabling the surface scanning of the examined material.*

[Engineering of Biomaterials 167 (2022) 17-23]

doi:10.34821/eng.biomat.167.2022.17-23

Submitted: 2023-04-12, Accepted: 2023-05-05, Published: 2023-05-15



Copyright © 2022 by the authors. Some rights reserved. Except otherwise noted, this work is licensed under <https://creativecommons.org/licenses/by/4.0>

*The quantitative results obtained facilitate an assessment of the internal structure and differentiation of cartilage based on its anatomical location (e.g., joints or ears). Direct images acquired during the examination offer insights into the internal structure of cartilage tissue, revealing morphological disparities and variations in intercellular spaces. The scans obtained during the measurements have unveiled substantial distinctions, particularly in the intercellular 'essence', characterized by granularities with a diameter of approximately 0.5  $\mu\text{m}$  in ear cartilage and structural elements in articular cartilage measuring about 0.05  $\mu\text{m}$ . Thus, AFM can be a valuable cognitive tool for observing biological samples in the biological sciences, particularly in medicine (e.g. clinical science).*

**Keywords:** atomic force microscopy, cartilage, biopolymers, chondrocytes, intercellular matrix

## Introduction

The tissue structures of the human body are composed of polymers that constitute mainly proteins, polysaccharides, glycosaminoglycans, and the biggest structural molecules, i.e. nucleic acids. The above-mentioned particles have a structure based on chemical bonds, predominantly covalent, ionized between elements, which determines (along with "genetic signpost") their functions - mostly in biochemical reactions or as a structural material. Different types of structures could also be observed in the human body, such as cartilage structures. These cartilages consist of polymers defined as protein molecules, e.g. collagen, elastin, or fibronectin. The histological diagrams of vitreous, fibrous, and elastic cartilages are presented in FIG. 1.

Cartilage is made up of cells called chondrocytes and a well-developed intercellular substance consisting of fibers and a basic substance called a matrix. Cartilage does not contain blood or lymphatic vessels and is not innervated. Apart from the articular surfaces, it is covered with well-vascularized, fibrous connective tissue. Depending on the structure of the intercellular substance and performed function, three types of cartilaginous tissue are distinguished: vitreous (type II collagen), fibrous (type I collagen), and elastic (a dense meshwork of elastic fibers) (FIG. 1). Laryngeal and articular cartilage are naturally cartilaginous, whereas auricular cartilage is elastic. The vitreous cartilage of the adult body constitutes most of the larynx cartilage, the cartilaginous trachea and bronchi rings, the cartilaginous parts of the ribs, the nasal septum, and covers the articular surfaces. Vitreous cartilage is a hard elastic tissue of a bluish-white color. The cartilage surface is covered by the perichondrium. Under the perichondrium is the subchondral zone containing spindle-shaped chondrocytes arranged in a few layers. These cells lie in cavities separated by a large amount of intercellular substance. Deep in cartilage, chondrocytes have a spherical shape; they are also larger and form groups called chondrons. The cells of a single chondron originate from the same parent cell and are called isogenic groups. Within the isogenic group, the chondrocytes are separated by the thin layer of the extracellular substance [2,3]. Chondrocytes are metabolically active cells that synthesize components of extracellular substances. They have one or two vesicular nuclei. The extracellular substance of vitreous cartilage is made up of collagen fibers and the basic substance (matrix). Collagen fibers account for about 40% of the dry cartilage mass.

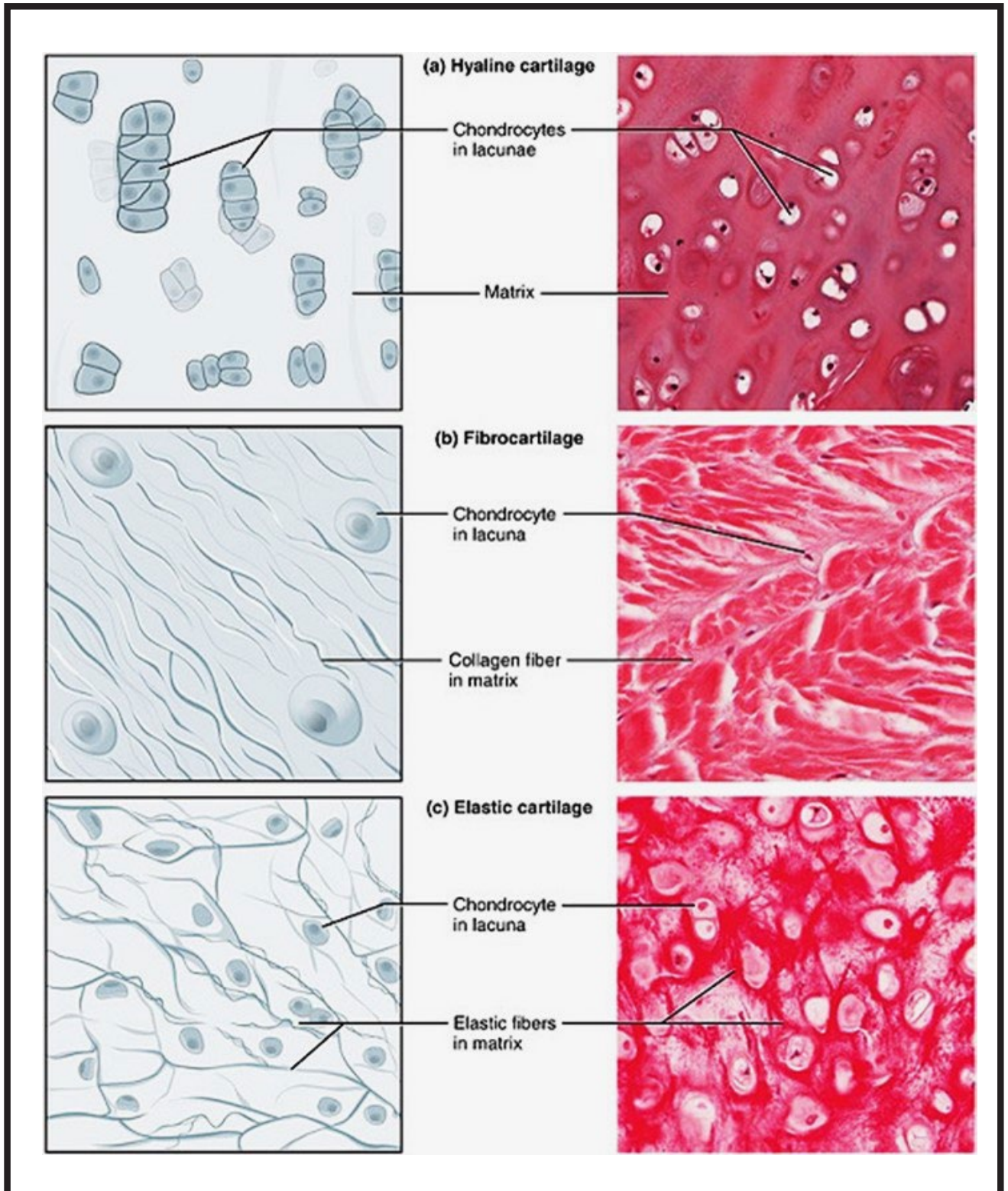


FIG. 1. Histological diagram of vitreous cartilage (a), fibrous cartilage (b), and elastic cartilage (C) [1].

Made up of type II collagen, they occur as thin fibers arranged in a dense, irregular network. The arrangement of collagen fibrils is more organized and in line with the direction of loads in vitreous articular cartilage. Due to their small diameter and the same refractive index as the basic substance covering them, the fibers are invisible in standard preparations. The main components of the basic substance include hyaluronic acid and proteoglycans, both of which influence cartilage hardness and elasticity. Elastic cartilage is found in the auricle, external auditory canal, auditory trumpet, epiglottis, and small cartilages of the larynx.

Its overall structure is similar to vitreous cartilage. The two- and three-celled chondrons found here are regularly distributed in a small amount of the intercellular substance. The distinguishing feature of elastic cartilage tissue is the presence of a dense meshwork of elastic fibers. The amount of collagen II fibrils is limited. Due to such a structure, deformed cartilage quickly returns to its previous shape. Elasticity and deformability are the main characteristics of elastic cartilage [4].

It is worth mentioning that contemporary research methods focusing on solid-state physics and material science can be used in qualitative and quantitative assessment at micro- and nanometric resolution of both natural and synthetic materials. According to the broad literature review, materials engineering has, in its cognitive arsenal, research techniques applied in analyzing materials of human origin that are at the borderline of biology and medicine. Available research methods allow for conducting complex studies at the molecular level and imaging techniques such as light microscopy, fluorescent microscopy, confocal microscopy, and advanced observations using electron microscopy, including cryogenic microstructure observations.

On the other hand, in the above-discussed research methods, synthetic materials pose a minor research problem. Regarding biological objects, the data found in the literature on the subject of biomedical/material engineering emphasize a wide use of scanning electron microscopy (SEM), scanning-transmission electron microscopy (STEM), and transmission electron microscopy (TEM), X-ray spectroscopy, Raman spectroscopy, time-of-flight secondary ion mass spectrometry (TOF-SIMS) and matrix-assisted laser desorption/ionization (MALDI-TOF). The literature on the subject also includes some reports on the use of atomic force microscopy (AFM) with nanoindentation and the discussed microscopic and spectroscopic observation methods using synchrotron beams in research into living matter. Currently, this situation, due to significant technological developments, is increasingly evolving and allows for performing previously unavailable measurements.

The authors of the presented research undertook the challenge of a mechanical and topographical examination of cartilaginous tissues. The discussed tissues are the macroscopic building blocks of the mammalian body (including human) with a functional relationship to bone, muscle, and fascial structures. Therefore, it is essential to gain the best possible understanding of their internal structures and differentiation. In the current stage of advanced technological development, one of the methods of investigating this issue is atomic force microscopy and related methods of assessing mechanical properties (e.g. nanoindentation).

## Materials and Methods

The research subjects were ear cartilage and articular cartilage (FIG. 2). The research material came from the Department of Normal Anatomy of the Silesian Medical University. The first step in sample preparation was sample drying at room temperature for seven days. The samples were then immersed in alcohol for the next seven days. After this time, the cartilages were sectioned into small, thin slices. The final stage was fixing the analyzed cartilages on a basal slide, as shown in FIG. 2.

Atomic force microscopy (AFM) analysis was performed using a HYSITRON TI950 TriboIndenter (Bruker, Billerica, MA, USA). It is an integrated system with three measurement heads: an atomic force microscope model AFM QScope™ 250, a nanoindenter, and a precision light microscope. It allows for examining a wide range of engineering materials and, to a limited extent, biological specimens. The area for AFM examination was selected based on the image obtained from the light microscope. Tribological cartilage testing was carried out using the Q-WM190 low-frequency tapping mode probe (tip-a) with a length of 225  $\mu\text{m}$ , an elastic constant of 48 N/m and a resonant frequency of 190 kHz. The results were processed using the manufacturer's software - Hysitron TriboScan and Quesant Atomic Scan SPM (FIG. 3).



FIG. 2. Cartilage preparations placed on a basic slide.

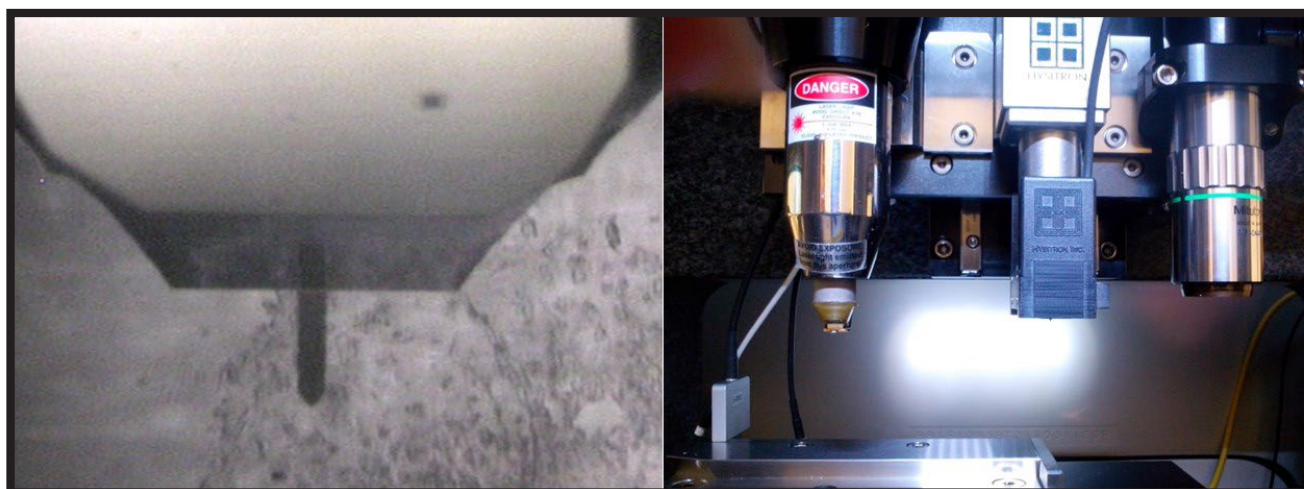


FIG. 3. View of the AFM Q-WM190 probe and measurement heads (AFM, nanoindentation, light microscope) included in the HYSITRON TI950 TriboIndenter.

In the atomic force microscopy technique, a scanning probe moves along the sample and measures at successive points whose distance from each other depends on the desired resolution [5-6]. The AFM method allows imaging of micro- and nanoscale structures in three dimensions (3D). Moreover, atomic force microscopy measurements can be carried out under varied environmental conditions, even when chemical reactions are performed. The measurements provide information on physicochemical and mechanical parameters such as roughness, frictional force values between the blade and the surface of the studied sample, adhesion forces, viscosity, and microhardness. It should also be underlined that the AFM technique allows for the characterization of biological materials [5-8]. The main advantages of the AFM method are the possibility of obtaining three-dimensional images at the nanoscale, the short measurement time, the resolution, and "in situ" measurements [5-8]. Moreover, during the AFM measurements, the three modes can be chosen (further in the text). The block diagram of the atomic force microscope is presented in FIG. 4. The essential elements of the atomic force microscope include a measuring head (containing, among others, a system for monitoring probe lever deflection and a piezoelectric scanning system), and a control unit directly connected to a computer. The operating principle of the microscope is based on the bending of the lever on which the probe (called the *tip*) is placed as a result of the activity of forces between the probe and the surface. As the probe is moved along the surface, the lever deflection is measured using a focused laser beam that strikes the photodetector after reflecting off the lever surface. Each deflection of the lever causes a change in the position of the laser spot on the detector, which makes it possible to determine the difference in the lever position with an accuracy of less than 1 nm. Changes in the position of the laser spot in the photoelement are converted into electrical impulses. Then the impulses are transformed, and transmitted to a computer, thus allowing for the registration of a force map for each point on the surface, which is processed into an image by the computer.

However, the image obtained from the microscope provides only part of the information received when the sample is scanned, since scanning can also provide additional information on its roughness [5]. An operating principle of the atomic force microscope is schematically presented in FIG. 5. The tip is situated on an elastic micro-lever whose deflection enables determining the interatomic interaction between the atoms of the tip and the studied surface. Movements of the probe lever are recorded using a deflected laser beam on a four-section photodetector, due to which the computer generates a topographic map of the analyzed surface [5].

From the measuring point of view, the atomic force microscope can operate in three modes: contact, non-contact, and tapping. In the contact mode, short-range interatomic interaction forces are used. The tip is in contact with the sample during scanning. The applied force on the surface ranges from  $10^{-11}$  N to  $10^{-7}$  N, which creates a thight contact area. During scanning, a probe with a low elastic constant ( $c < 1$  N/m) minimizes the interaction force between the tip and the sample. The force is measured by recording the deflection of the free end of the lever with the tip during the scanning.

On the other hand, the contact mode is characterized by the possibility to obtain high-resolution images due to the increased adhesion forces caused by surface contamination. However, the possibility of damage to the sample or the tip is high. Non-contact imaging uses magnetic, electrostatic, and van der Waals forces. The distance of the tip from the sample ranges from 1 to 10 nm. The lever length is approximately 100-200  $\mu\text{m}$ , and the response to the force acting on it changes the amplitude and vibration frequency, which provides the information needed to register an image. However, compared to the contact mode, it allows obtaining images with lower resolution.

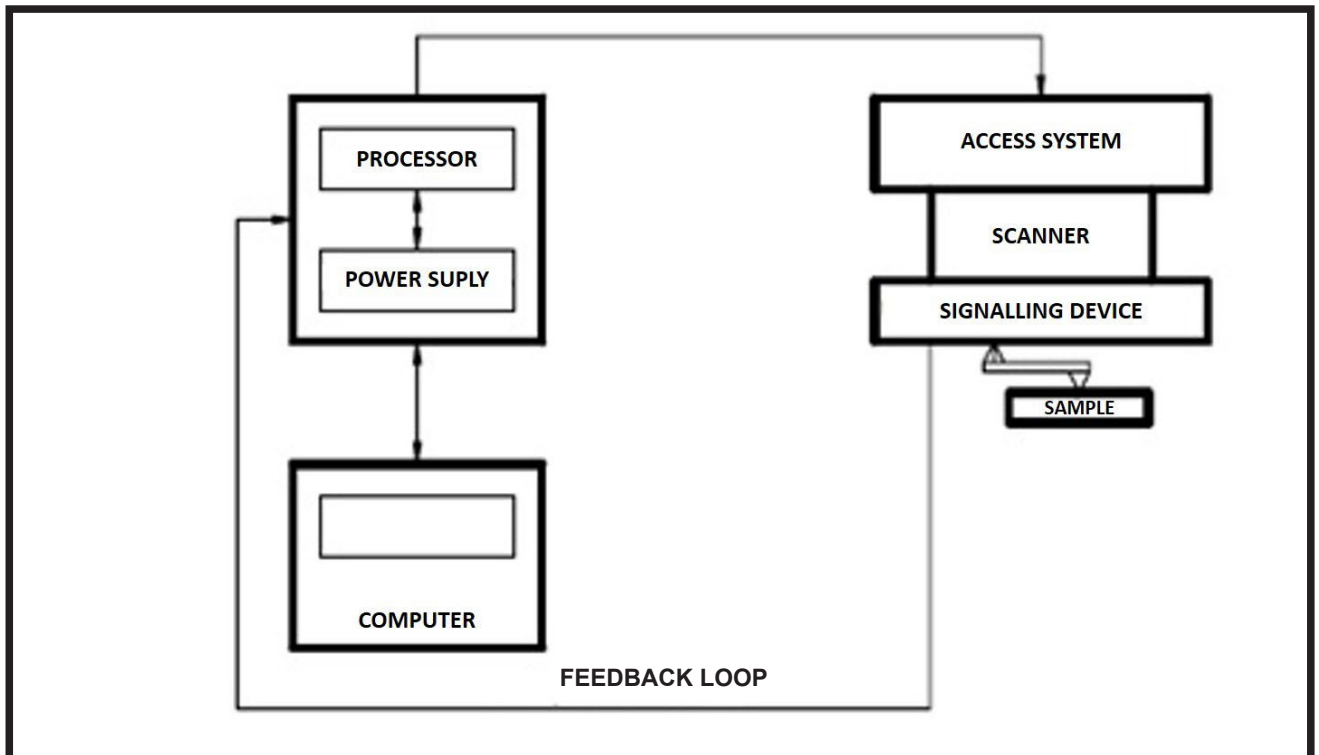


FIG. 4. Block diagram of the atomic force microscope [6].

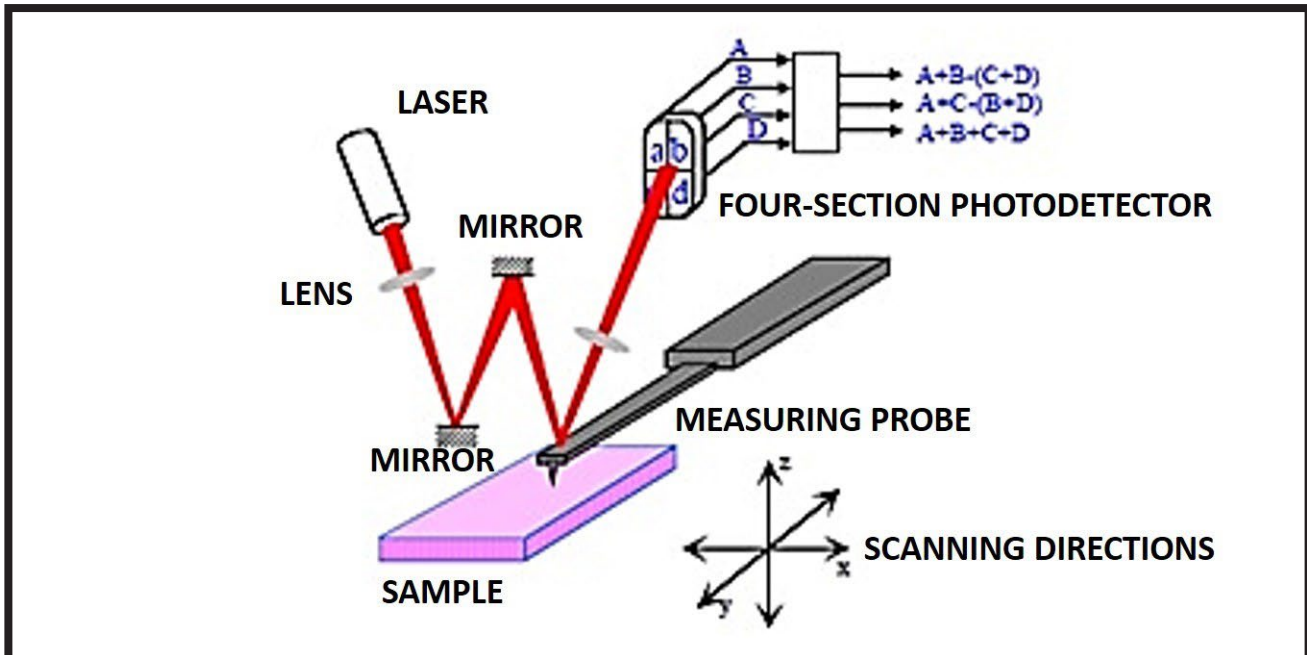


FIG. 5. Scheme illustrating the operating principle of the atomic force scanner [6].

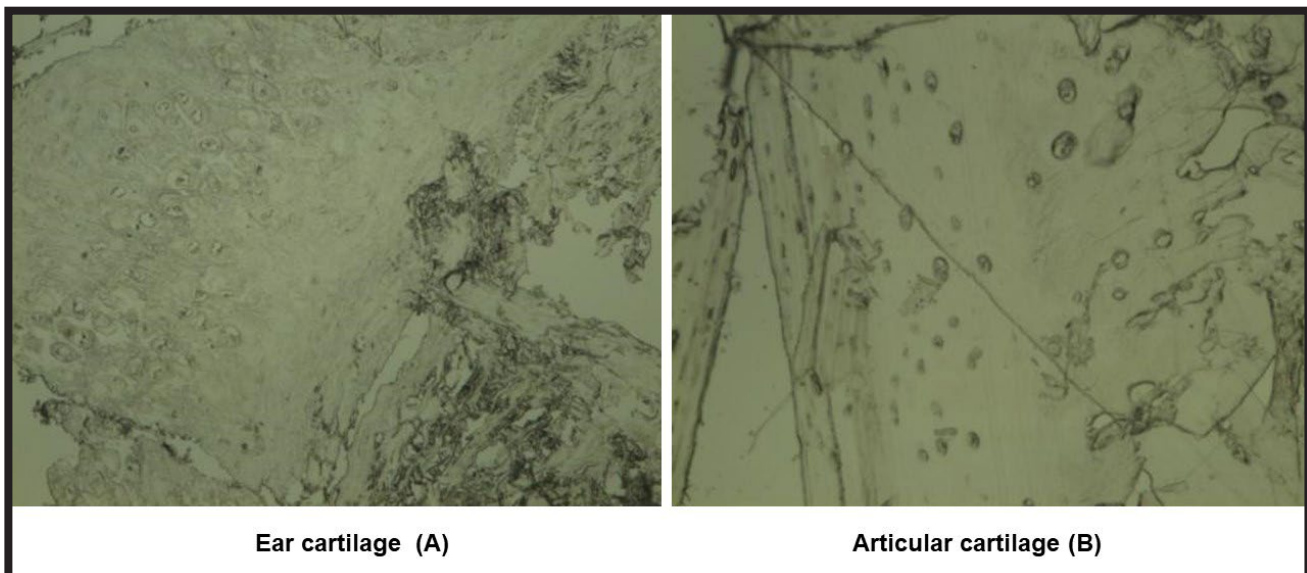


FIG. 6. Microstructure images of ear cartilage (A) and joint (B) collected using a light microscope.

In tapping mode, both long-range and short-range forces are used to obtain the image. Scanning the surfaces of the “soft” materials is also possible since no damage is done to the scanned surfaces. This mode needs a high spring constant of the lever (20-80 N/m) and its high resonance frequency (200-400 kHz). The oscillation amplitude is significant at >20 nm, while the tip has no contact with the sample. The tapping contact mode is also characterized by good resolution, as in the case of the contact mode. During scanning of the sample in the tapping mode, information from the surface morphology, roughness, adhesion, and hardness is provided.

## Results and Discussion

FIG. 6 shows images recorded using a light microscope of the ear and articular cartilage tissue, respectively. As can be seen, the elastic cartilage specimen from the ear (FIG. 6A) contains a significant density of chondrocytes distinct from a large amount of extracellular substance and forms isogenic groups in places. A different nanostructure was observed in the articular cartilage (FIG. 6B), classified as vitreous cartilage.

The microstructure image shows that the density of the chondrocytes is relatively low and that they occur as single cells, not as groups. Besides, in addition to individual chondrocytes, there is a large amount of extracellular substance in the examined material.

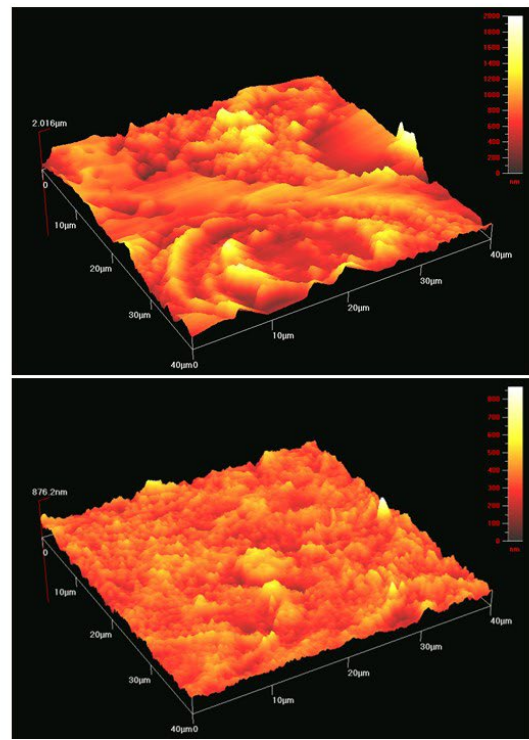
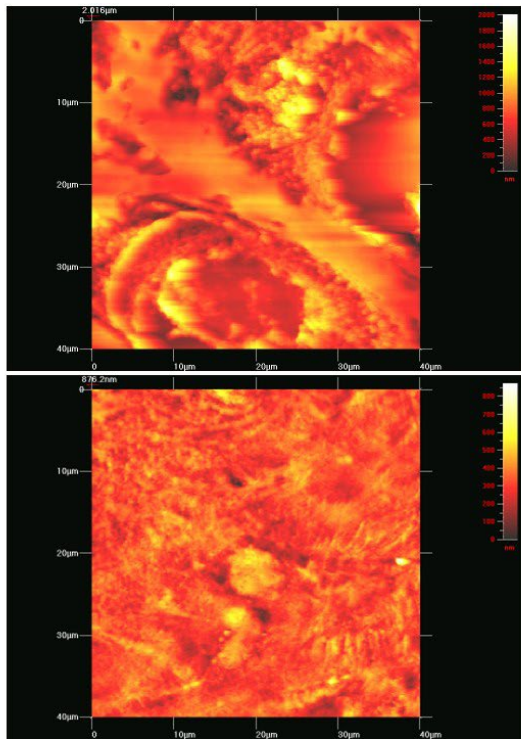


FIG. 7. AFM scan images for ear cartilage in 2D and 3D. The top image shows two chondrocytes, and the bottom shows the extracellular matrix.

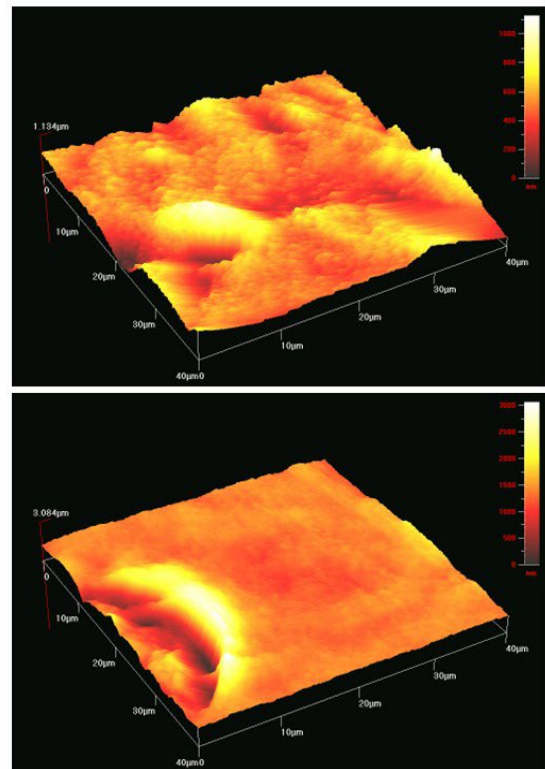
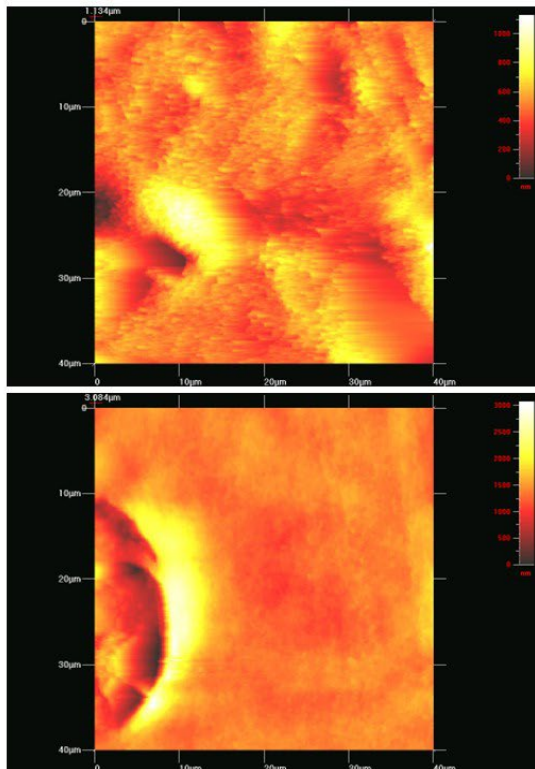


FIG. 8. AFM scan images for articular cartilage in 2D and 3D. The top image shows the extracellular matrix and the bottom image shows a single chondrocyte.

For better visualization of the ear cartilage structure at high-resolution, 2D and 3D AFM surface topography scans were performed (FIG. 7). Obtained images revealed the complex structure of ear cartilage. Additionally, 2D and 3D images clearly showed the typical cellular structure of elastic cartilage, where chondrocytes lie close to each other. The chondrocyte is clear and significantly distinct from the extracellular matrix. The cell depths range from 0 to 2,000 nm, while the matrix depth is no higher than 600 nm.

Similar high-resolution, 2D and 3D visualization of the microstructure of studied articular cartilage is presented in FIG. 8. Nanostructure images of articular cartilage (vitreous cartilage) presented a negligible proportion of chondrocytes as the building block of this type of tissue. As it can be seen, there is a predominance of the extracellular matrix whose depth, like in the case of ear cartilage, is about of 600 nm. On the other hand, the clustered chondrocytes found in elastic cartilage and the chondrocytes in vitreous tissue are much more separated from the matrix, with depths of up to 4,000 nm. What is also worth mentioning is a different type of intercellular matrix in which defined fibrous structures (collagen fibers) are found. It is much more compact and smoother compared to ear cartilage.

## Conclusions

In the presented work, the atomic force microscopy (AFM) technique was used to characterize the surface of the ear and articular cartilages in 2D and 3D, respectively. Based on the recorded 3D images, it can be seen that both studied cartilages were built from the intercellular matrix and chondrocytes (two chondrocytes for ear cartilage and a single chondrocyte for articular cartilage). The depth differences between the intercellular matrix and chondrocytes were also observed and measured. It was revealed that the depth of the intercellular matrix for the investigated cartilages was lower than 600 nm. Depth measurements of chondrocytes showed that for articular cartilage was higher (about 4,000 nm) in comparison to the ear cartilage (about 2,000 nm).

As one of the research methods applied in natural and synthetic materials engineering, the atomic force microscopy technique also can be used in biological and medical sciences. The main advantages of the AFM include:

- possibility of the observation of biological objects that do not require complex or challenging sample preparation process, as in the case of electron microscopy methods (SEM, STEM, TEM, cryo-EM),

- absence of changes caused by object preparation in the structure of the studied material, e.g. the use of fixatives and dehydration,
- low costs of preparation and methodology of the conducted measurements,
- the scanning modes of the surfaces of the observed objects generate high-resolution, three-dimensional visualization images combined with precise mapping of depth and height shown on the color change scale,
- precise comparison of the structures of individual tissues on a nanometric scale, with mapping of the smallest differences occurring in the cells (chondrocytes) and the surrounding space (extracellular matrix),
- morphological differentiation of the extracellular matrix with nanometric resolution allowing to assign the object according to its origin (joint, ear).

Moreover, the obtained research tasks revealed their innovative and applied character from the scientific perspective on the borderline of biomedical and material engineering, biology, and medicine. Particular emphasis should be placed on the usefulness of the AFM technique in understanding and differentiating human cartilage structures, e.g. in terms of its morphology and nanostructure.

The obtained research findings reveal the potential for future use of atomic force microscopy as a diagnostic tool in transplantology.

## Acknowledgements

*Research financed by the project PCN-1-082/K/0/O (Medical University of Silesia in Katowice).*

## ORCID iD

J. Paluch:	 <a href="https://orcid.org/0000-0001-7675-0623">https://orcid.org/0000-0001-7675-0623</a>
J. Markowski:	 <a href="https://orcid.org/0000-0003-3416-7354">https://orcid.org/0000-0003-3416-7354</a>
J. Pilch:	 <a href="https://orcid.org/0000-0001-6792-0985">https://orcid.org/0000-0001-6792-0985</a>
W. Smółka:	 <a href="https://orcid.org/0000-0003-4074-9705">https://orcid.org/0000-0003-4074-9705</a>
K.P. Jasik:	 <a href="https://orcid.org/0000-0003-3974-6507">https://orcid.org/0000-0003-3974-6507</a>
F. Kilian:	 <a href="https://orcid.org/0000-0002-2658-1451">https://orcid.org/0000-0002-2658-1451</a>
W. Likus:	 <a href="https://orcid.org/0000-0002-4738-6102">https://orcid.org/0000-0002-4738-6102</a>
G. Bajor:	 <a href="https://orcid.org/0000-0002-7195-8422">https://orcid.org/0000-0002-7195-8422</a>
D. Chrobak:	 <a href="https://orcid.org/0000-0003-1766-1350">https://orcid.org/0000-0003-1766-1350</a>
K. Glowka:	 <a href="https://orcid.org/0000-0002-1889-5557">https://orcid.org/0000-0002-1889-5557</a>
O. Starczewska:	 <a href="https://orcid.org/0000-0002-7659-2909">https://orcid.org/0000-0002-7659-2909</a>

## References

- [1] <http://www.differencebetween.net/science/health/difference-between-hyaline-cartilage-and-elastic-cartilage/>
- [2] Zabel M.: Histologia - podręcznik dla studentów medycyny i stomatologii, Wydawnictwo medyczne Urban & Partner, Wrocław (2005).
- [3] Malejczyk J.: Budowa i immunologia tkanki chrzęstnej, Acta Clinica 1 (1) (2001) 15-22.
- [4] Sawicki W.: Histologia, Wydawnictwo Lekarskie PZWL, Warszawa (2005).
- [5] Rymuza Z.: Advanced techniques for nanotribological studies, Scientific Problems of Machines Operation 1 (161) (2010) 33-43.
- [6] Bramowicz M., Kłysz S.: Zastosowanie mikroskopii sił atomowych (AFM) w diagnostyce warstwy wierzchniej, Zeszyty naukowe ITWL, zeszyt 22 (2007) 159-166.
- [7] Gotszalk T.P.: Systemy mikroskopii bliskich oddziaływań w badaniach mikro i nanostruktur, Oficyna Wydawnicza Politechniki Wrocławskiej (2004).
- [8] Ilnatouski M., Pauk J., Karev D., Karev B.: AFM-Based Method for Measurement of Normal and Osteoarthritic Human Articular Cartilage Surface Roughness, Materials 13 (2020) 2302.

## MATERIALS BASED ON CHITOSAN ENRICHED WITH ZINC NANOPARTICLES FOR POTENTIAL APPLICATIONS ON THE SKIN

KAROLINA KULKA<sup>1\*</sup> , ANDŻELIKA SZMEJKOWSKA<sup>1</sup> ,  
ALINA SIONKOWSKA<sup>1</sup> , MAGDALENA WYPIJ<sup>2</sup> ,  
PATRYCJA GOLIŃSKA<sup>2</sup> 

<sup>1</sup> DEPARTMENT OF BIOMATERIALS AND COSMETIC CHEMISTRY, FACULTY OF CHEMISTRY, NICOLAUS COPERNICUS UNIVERSITY IN TORUŃ, GAGARINA 7, 87-100 TORUŃ, POLAND

<sup>2</sup> DEPARTMENT OF MICROBIOLOGY, FACULTY OF BIOLOGICAL AND VETERINARY SCIENCES, NICOLAUS COPERNICUS UNIVERSITY IN TORUŃ, LWOWSKA 1, 87-100 TORUN, POLAND

\*E-MAIL: KKULKA@DOKTORANT.UMK.PL

### Abstract

*Chitosan as a nontoxic, biodegradable, and biocompatible biopolymer with film-forming properties can also be modified to improve its parameters. Modification of polymer films by the addition of nanoparticles is an increasingly common solution due to the higher efficiency of products at the nanoscale compared to the macroscale. In this work, thin chitosan films enriched with biogenic zinc oxide nanoparticles (ZnONPs) from *Fusarium solani* IOR 825 were obtained by the solvent evaporation method. The influence of nanoadditive on the physicochemical, mechanical, and antimicrobial properties of the polymeric matrix was evaluated. Two different concentrations of ZnONPs were added to the chitosan solution. Spectrometric measurements, mechanical tests, microscopic imaging, and microbiological tests were performed for nanoparticles-modified and control samples. Analysis revealed that ZnONPs influence the properties of chitosan films. FTIR spectroscopy showed changes that are the result of interactions between polymer matrix and the additive. Modified samples were characterized by increased values of Young's modulus and tensile strength. SEM analysis combined with energy-dispersive X-ray spectrometry confirmed the presence of zinc in the modified films. The addition of nanoparticles slightly affected the surface morphology of the tested samples, and an increase in roughness was observed. Microbiological tests showed the biostatic activity of the films containing ZnONPs. The obtained films based on chitosan with the addition of ZnONPs can be considered easy-to-obtain biomaterials with potential use as cosmetic and biomedical products.*

**Keywords:** chitosan, zinc oxide nanoparticles, polymer films, antimicrobial activity

## Introduction

Chitosan is a well-known biopolymer with valuable physicochemical and biological properties. It is a chitin derivative that is soluble in dilute acid solutions. It is biodegradable and biocompatible, nontoxic, and has film-forming properties, as well as antioxidant and antimicrobial activity [1,2]. The source of chitosan is usually marine organisms, but also fungi and insects. Chemical or enzymatic deacetylation of chitin results in a product composed of  $\beta$ -glucosamine and N-acetylglucosamine units. Depending on the process parameters used and the quality of the starting material, a product with a different degree of deacetylation (DD) and a different molecular weight can be obtained.

Skin applications of chitosan are important, especially in cosmetic and biomedical fields. The biological activity of chitosan includes antioxidant and antimicrobial effects, as well as anti-inflammatory properties [3,4]. The antioxidant properties are the result of the presence of free functional groups (amino, amino acetyl, and hydroxyl groups) in the polymeric chain. These groups can react with reactive oxygen and nitrogen species [5]. In cosmetic formulations, it acts as an emulsion stabilizer and thickener, and thanks to its antimicrobial activity, it can reduce the number of preservatives used. In addition, it has a beneficial effect on skin and hair, moisturizing them and preventing the loss of water through the creation of an occlusive layer. Chitosan not only improves the condition of the skin in terms of care but can also help in wound treatment. It is typically used in dermatology in the form of active dressing. There are several stages in the wound healing process: hemostasis, inflammation, proliferation, and remodeling [6]. Chitosan-based active dressing participates in three phases of this process. First of all, its polycationic molecules bind to negatively charged thrombocytes and erythrocytes, supporting the blood coagulation process [3,6]. In the next step, it helps fight inflammation by cleansing the wound of bacteria. The last phase involves stimulating the production of granulation tissue, which accelerates skin proliferation [6]. Additionally, it helps to maintain good wound moisture and can easily absorb exudate [3].

Chitosan can be used in many different forms, but for applications on the skin, the film form seems to be one of the best choices. The film-forming properties of this carbohydrate polymer are extremely useful in products for surface applications, particularly in the biomedical, cosmetic, food, and packaging industries. Depending on the application, the mechanical properties of such films are important. Chitosan-based films are often characterized by relatively low tensile strength and brittleness, while cross-linking improves these properties [7,8]. Modifications of chitosan films are carried out not only to improve mechanical properties but also to obtain a material with completely new activity, such as biological. In chitosan-based products for biomedical or food applications, additives are often used to increase the antimicrobial potential, e.g. drugs, zinc oxide, or essential oils [9-12]. Lian et al. obtained chitosan/starch films incorporated with zinc oxide nanoparticles (ZnONPs) and the results of their work showed positive antibacterial activity on *S. aureus* and *E. coli* compared to the pure films [13].

[Engineering of Biomaterials 167 (2022) 24-31]

doi:10.34821/eng.biomat.167.2022.24-31

Submitted: 2023-04-22, Accepted: 2023-05-24, Published: 2023-05-30



Copyright © 2022 by the authors. Some rights reserved.  
Except otherwise noted, this work is licensed under  
<https://creativecommons.org/licenses/by/4.0>

The use of nanoadditives has recently become widely applied in various fields, including the one discussed. Nanotechnologies involve precise molecular and atomic precision techniques, and nanotechnology products exhibit two key characteristics: at least one dimension within the range of 1-100 nm and properties dependent on the characteristic dimension. Nanostructures often demonstrate distinct physicochemical properties compared to their macroscale counterparts, encompassing chemical, optical, mechanical, or magnetic traits [14]. Among nanoparticles (NPs), different groups can be distinguished, such as metallic NPs, ceramic NPs, and polymeric NPs [15]. At the nanoscale, numerous materials can readily interact with biomolecules at cellular and subcellular levels, making biomedical applications a specialized domain for nanotechnology products. Metal nanoparticles, notably silver (AgNPs) or zinc oxide nanoparticles (ZnONPs), are one of the most interesting for enhancing polymer films with nanoadditives [16-20]. The purpose of incorporating such additives is to enhance mechanical properties, boost antimicrobial activity, and improve parameters like conductivity and water retention capacity [18,19]. These parameters are particularly vital for dressing products and food packaging.

### Comparison of zinc on a macro and nanoscale

Zinc, with an atomic number of 30, is a naturally occurring element. It presents as a brittle metal with a blue-white hue, possesses relatively low melting and boiling points, reacts with acids and bases, and undergoes passivation in the air [21]. In living organisms, it functions as with multifaceted role. Within the human body, zinc contributes to skin regeneration, the proper functioning of the cardiovascular system, and plays vital roles in immune and metabolic mechanisms. Several functions of zinc arise from its role as a cofactor of enzymes with antioxidant activity and its involvement in DNA transcription ('zinc fingers'), cell proliferation and differentiation, and more [22,23]. Approximately 2 g of zinc are distributed throughout the entire human body, with the highest concentrations found in skeletal muscle, bone, skin, brain, and kidney, in descending order. In its natural state, zinc is not found in free form but primarily exists as zinc oxide, zinc carbonate, and zinc sulphide [21].

Zinc nanoparticles exhibit antimicrobial, photocatalytic, and radioprotective properties. Due to their increased surface area-to-volume ratio, nanoparticles display distinct reactivity, making them more reactive than bulk materials. This heightened reactivity is desirable for applications such as antimicrobial purposes. However, in other applications like radioprotective formulations, may pose a risk to the user due to possible phototoxic effects [24]. Zinc ions are essential for cells function but become harmful at higher concentrations. Nanoformulated zinc appears to be a more effective antibacterial agent than traditional forms of zinc [25]. The antibacterial mechanism may involve the release of ions that penetrate cells and induce toxicity [25] or the production of reactive oxygen species that breach microorganism cell membrane and cause bacterial death [26]. In addition, zinc nanoforms operate through a distinct mechanism compared to conventional antibiotics, making them more effective against resistant strains [26]. Concerning the enhancement of antibacterial activity through the addition of ZnONPs to chitosan films, the mechanism may involve electrostatic interactions between the positively charged amino groups of chitosan and the negatively charged bacterial cell wall, facilitating the penetration of zinc ions [13]. Furthermore, the incorporation of zinc oxide nanoparticles into the biopolymer matrix can enhance its structural integrity, creating a more compact structure.

The method of nanoparticle synthesis significantly impacts their physicochemical properties [27]. Three main methods can be distinguished for the synthesis of nanoparticles: chemical, physical, and biological [14,21]. In recent years, biological methods, considered environmentally friendly alternatives, have gained popularity. Biogenic nanoparticles, in contrast to chemically and physically synthesized ones, are believed to be less toxic because their synthesis does not require toxic reagents or high energy consumption and stabilization process, which often use toxic reagents, and do not produce toxic wastes. To stabilize biogenic nanoparticles, they are coated with biomolecules of natural origin [28,29]. Microorganisms, plant extracts, or enzymes are used as substrates in these methods [30,31].

In the present study, we investigated the effect of the addition of mycogenic ZnONPs on the properties of films prepared from low molecular weight chitosan. A series of tests were carried out to characterize the polymer films obtained, including microscopic analysis, infrared spectroscopic analysis, and microbiological studies. The use of different nanoparticle concentrations was compared.

## Materials and Methods

### Materials

Low molecular weight chitosan ( $M_v = 7.74 \cdot 10^5$  (g/mol), deacetylation degree 82.90%) was purchased from the POL-AURA company (Dywit, Poland). Glycerol, acetic acid, zinc sulphide, and sodium hydroxide were acquired from POCH (Gliwice, Poland).

### ZnONPs synthesis

Zinc oxide nanoparticles (ZnONPs) were synthesized using a fungal extract from *Fusarium solani* IOR 825,  $ZnSO_4$ , and NaOH in a ratio of 1:1:1 (v/v/v) and heated for 15 min at 40°C. They were further characterized for physical and chemical activities, as previously described by Trzcińska-Wencel et al. [29].

### Preparation of initial solution

2% (w/v) solution of chitosan (CS) was prepared in 0.1 M acetic acid. The mixture was stirred on a magnetic stirrer until complete dissolution.

### Preparation of chitosan films

Films were obtained using a solvent evaporation method. A 30 g of chitosan solutions were weighed out and 1% (w/w) of glycerol (G) was added to each solution. The solutions thus prepared were stirred for 3 h. Glycerol (G) was used as a plasticizer. After stirring, one solution with glycerol was poured onto a polystyrene plate (10 x 10 cm) as well as a pure chitosan solution. 0.1% (w/w) and 0.2% (w/w) ZnONPs in powder form were added to subsequent solutions with glycerol, respectively. The solutions were stirred to dissolve the additive and then poured onto polystyrene plates (10 x 10 cm). The solution with 0.2% additive was additionally homogenized before pouring. They were left at room temperature to dry completely.

### FTIR spectroscopy

The interactions between the polymer and the additive were evaluated by Fourier transform infrared spectroscopy (FTIR) using Nicolet iS10 equipment with an ATR (attenuated total reflection) accessory and a diamond crystal (Thermo Fisher Scientific, Waltham, MA, USA). All spectra were recorded in absorption mode, with a resolution of  $4\text{ cm}^{-1}$  with 64 scans.

### Mechanical properties

Mechanical tests were carried out using a mechanical testing machine (Z.05, Zwick and Roell, Ulm, Germany). Young Modulus, tensile strength, and elongation at break were evaluated. The samples were cut in the shape of paddles (width 4 mm in the center). The parameters of the test program were as follows: the speed starting position was 50 mm/min, the speed of the initial force was 5 mm/min, and the initial force was 0.1 MPa. Data were collected using the TestXpert II 2017 program and the results were presented as average values with standard deviation.

### Scanning electron microscopy (SEM-EDX)

Surface imaging of the tested polymer samples was carried out using a scanning electron microscope (SEM) manufactured by LEO Electron Microscopy Ltd. (Model 1430 VP). In addition, an EDX Quantax 200 X-ray spectrometer with a Bruker AXS XFlash 4010 detector was used for spot analysis of the chemical composition of the samples to confirm the presence of zinc.

### Atomic force microscopy (AFM)

The polymer samples were analyzed using atomic force microscope (MultiMode Scanning Probe Microscope NanoScope IIIa; Digital Instruments Veeco Metrology Group, Santa Barbara, CA).

### Microbiological tests

The antimicrobial activity study of chitosan films with the additive of biogenic ZnONPs was performed using the diffusion method against selected strains of bacteria: *Escherichia coli* ATCC 8739, *Escherichia coli* ATCC 25922, *Klebsiella pneumoniae* ATCC 700603, *Listeria monocytogenes* PCM 2191, *Pseudomonas aeruginosa* ATCC 10145, *Salmonella enterica* PCM 2565, *Salmonella infantis* SES, *Staphylococcus aureus* ATCC 25923, *Staphylococcus aureus* ATCC 6538, and yeasts of *Candida albicans* ATCC 10231.

Strains were purchased from the American Type Culture Collection (ATCC; Manassas, Virginia, United States), the Polish Collection of Microorganisms (PCM; Wrocław, Poland), or obtained from Sanitary-Epidemiology Station (SES) in Toruń, Poland. Briefly, the films were cut into  $10 \times 10\text{ mm}$  pieces and placed on the surface of tryptic soy agar (TSB, Becton Dickinson, USA) in the Petri plates inoculated with microorganisms. Microbial inoculum was prepared from strain grown in tryptic soy broth (TSB, Becton Dickinson, USA) for 24 h at  $35^\circ\text{C} \pm 2^\circ\text{C}$  under shaking conditions at 120 r.p.m. Culture was used to prepare microbial suspension in sterile deionized water at a density of 0.5 units on the McFarland scale ( $1.5 \cdot 10^8\text{ CFU mL}^{-1}$ ) measured using a densitometer (Biosan, Latvia). The microbial inoculum was diluted with sterile deionized water to final concentrations of  $1.5 \cdot 10^5\text{ CFU mL}^{-1}$  before spreading onto the TSA medium in the Petri plates using a sterile swab. The plates with placed films were incubated for 24 h at  $37^\circ\text{C}$  and evaluated for antimicrobial activity.

## Results and Discussions

### Physicochemical properties

Chitosan films for testing were obtained using the solution casting method. After drying, the obtained films were easily removed from the plate. Control samples and the sample with 0.1% ZnONPs additive were smooth and homogeneous, whereas the film with 0.2% additive showed lumps (FIG. 1).

The spectra of pure chitosan samples and films with additives are presented in FIG. 2. The FTIR spectrum obtained for a pure sample of chitosan is characteristic of this polysaccharide, showing four main bands with the highest intensity. The broad visible band with a maximum at  $3355\text{ cm}^{-1}$  comes from the O-H and N-H stretching vibrations, which overlap. In addition, this band is the result of intramolecular hydrogen bonding of chitosan molecules [32]. The bands at about  $3400\text{ cm}^{-1}$  may additionally indicate the presence of water in the tested samples [33]. The band at  $2868\text{ cm}^{-1}$  confirms the presence of C-H bonds from  $-\text{CH}_3$  and  $-\text{CH}_2$  groups. The bending vibration coming from the N-H group appears at a wavelength of  $1653\text{ cm}^{-1}$ . In the  $1200\text{--}1000\text{ cm}^{-1}$  spectral region, vibrations of the C-O-C groups can be observed, confirming the presence of the O-glycosidic bond. The  $1200\text{--}900\text{ cm}^{-1}$  region is typical of polysaccharides and represents stretching vibrations of C-C and C-O bonds and C-H bending vibrations [32].

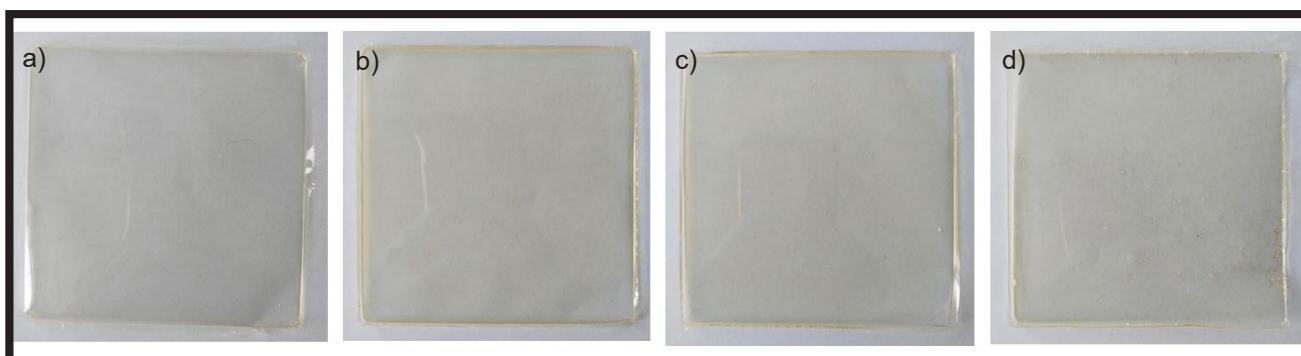


FIG. 1. Pictures of chitosan films: a) chitosan film (CS); b) chitosan film with 1% glycerol (CS/G); c) chitosan film with 1% glycerol and the addition of 0.1% zinc oxide nanoparticles (CS/G+ZnONPs(0.1%)); d) chitosan film with 1% glycerol and the addition of 0.2% zinc oxide nanoparticles (CS/G+ZnONPs(0.2%)).

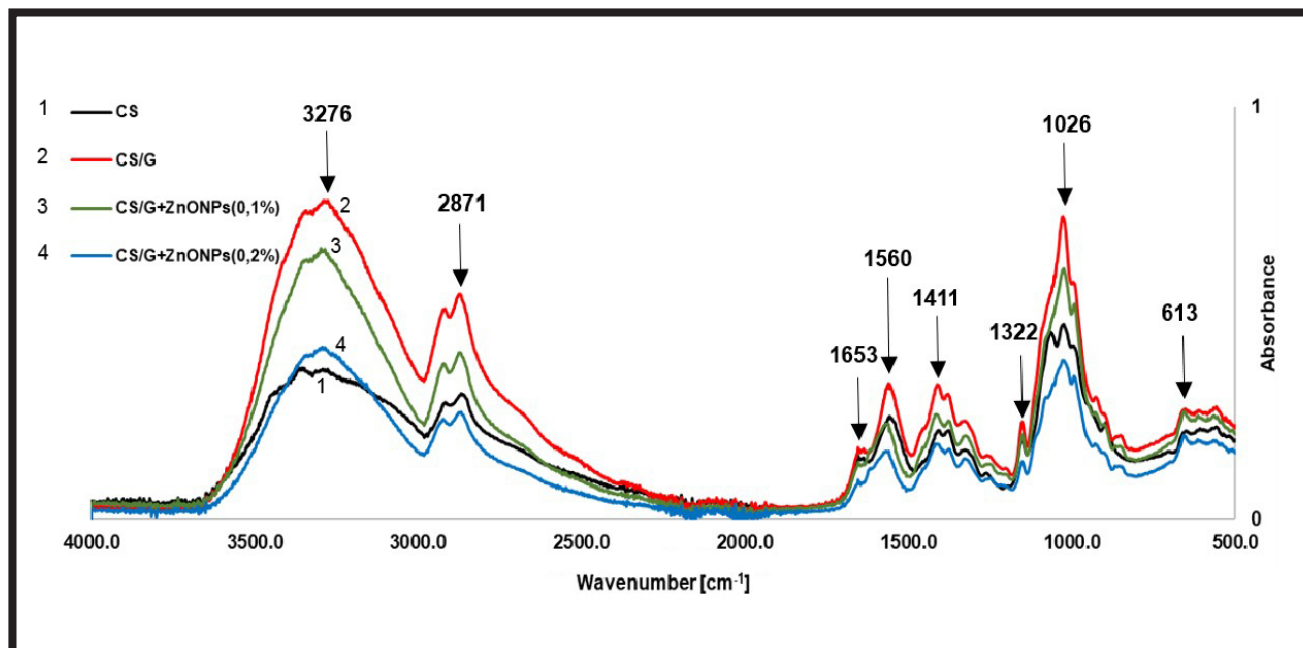


FIG. 2. IR spectra of polymer films.

Interactions that occur in a particular system can be uniquely reflected in the wavelengths present for the peaks in the spectrum [34]. The FTIR spectrum for the sample with the plasticizer added is similar to the spectrum of the original sample in terms of the appearance of individual bands. However, the intensity of the bands has been changed and a significant increase can be observed. First of all, the increased intensity of the bands around  $3200\text{--}3500\text{ cm}^{-1}$  and the sharpening of the peak indicate the interaction of the polymer with the plasticizer, in particular the formation of many new intermolecular hydrogen bonds. Small shifts were observed from  $3355\text{ cm}^{-1}$  (for the initial sample) to  $3276\text{ cm}^{-1}$  (sample with the addition of the plasticizer - glycerol), confirming that the addition of glycerol promotes the formation of hydrogen interactions in the tested system [32].

IR spectra for samples with the addition of ZnONPs show significant changes in the intensity of individual bands. These changes correspond to the amount of nanoparticles added; the higher the concentration of additive, the lower the intensity of the bands. In the case of the band corresponding to the  $\text{-OH}$  and  $\text{-NH}_2$  groups, this can be explained by the reduction of existing hydrogen bonds with the introduction of nanoparticles into the chitosan matrix [18,35]. The formation of new hydrogen bonds between the matrix and zinc oxide is indicated by slight shifts at a wavelength of about  $3300\text{ cm}^{-1}$ .

Changes for samples with the addition of nanoparticles in the band  $560\text{--}619\text{ cm}^{-1}$  confirm the presence of ZnO, reflecting the Zn-O stretching vibrations [18,36]. The positions of individual bands are presented in TABLE 1.

TABLE 1. Wavenumbers in IR spectra that occur in chitosan films with and without additives.

Functional group vibrations	Wavenumber [ $\text{cm}^{-1}$ ]			
	CS	CS/G	CS/G+ZnONPs(0.1%)	Ch/G+ZnONPs(0.2%)
O-H stretching	3355	3276	3359	3292
N-H stretching	3355	3276	3359	3292
C-H stretching	2868	2871	2971	2868
N-H bending	1653	1653	1649	1653
amide II C=O	1556	1560	1565	1568
O-H deformational	1407	1411	1415	1416
C-N stretching	1326	1322	1326	1328
C-O-C stretching	1024	1026	1024	1025
Zn-O	-	-	613	614

### Mechanical properties

The results of the tensile tests of thin chitosan films prepared with and without additives are shown in FIG. 3 and TABLE 2. It can be seen that the addition of glycerol and ZnONPs has a significant effect on the parameters tested.

Films with glycerol are characterized by a much lower Young's modulus value compared to pure chitosan films. The same applies to the tensile strength. Glycerol films are much more flexible and achieve a higher value of elongation at break. The use of a plasticizer (glycerol) allowed the nanoparticle films to be completely removed from the polystyrene plates and analyzed.

The addition of ZnONPs affects the properties of the chitosan-based film. The samples become more brittle, which is reflected in the values of the parameters tested, especially in the increase in the value of the Young modulus. It can be observed that the higher the additive content, the higher the tensile strength and the lower the elongation at break.

### Surface morphology

The surface morphology was studied by SEM-EDX and AFM. SEM and AFM pictures of the obtained films are shown in FIG. 4. EDX analysis was carried out to study the elemental composition of the films and to confirm the presence of zinc in the films. This analysis showed a homogeneous distribution of the elements in the film, indicating that the solutions were well mixed before the films were obtained (FIG. 5).

It can be observed that all films, both without and with additives, have a uniform structure with a fairly smooth surface morphology. The pure chitosan film (without additive) has a low roughness parameter. The presence of zinc nanoparticles in 0.1% concentration increases the roughness of the sample. This parameter is also influenced by the addition of glycerol (plasticizer) (TABLE 3).

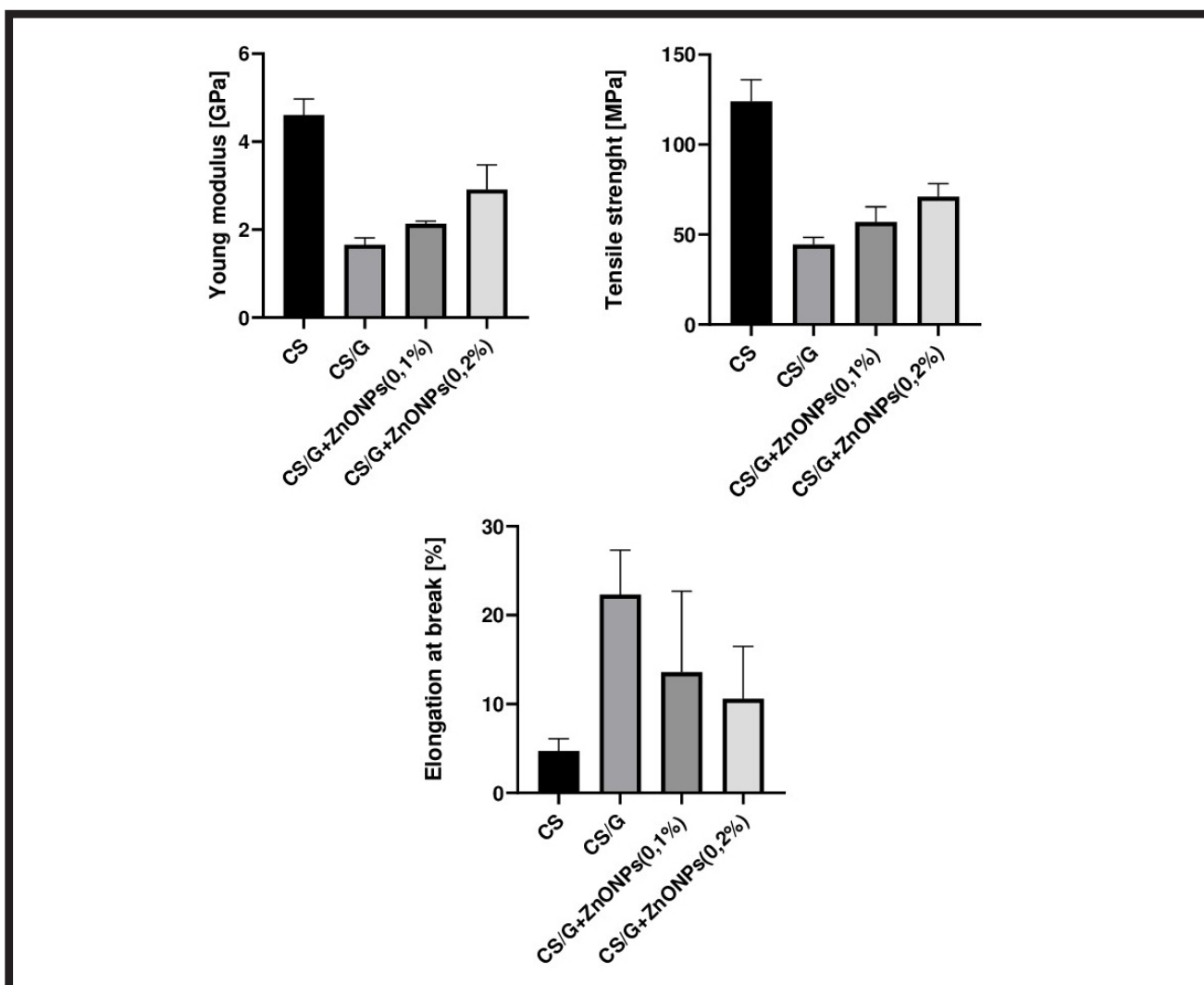


FIG. 3. Mechanical properties of chitosan films; error bars represent standard deviation (SD).

TABLE 2. Mean values of the mechanical parameters of the chitosan films with standard deviation (SD).

Parameter	CS	CS/G	CS/G+ZnONPs(0.1%)	CS/G+ZnONPs(0.2%)
Young Modulus [GPa]	4.61 ± 0.37	1.66 ± 0.16	2.13 ± 0.06	2.91 ± 0.56
Tensile strength [MPa]	124 ± 12.10	44.40 ± 3.96	56.90 ± 8.47	71.10 ± 7.24
Elongation at break [%]	4.70 ± 1.40	22.3 ± 5.00	13.60 ± 9.10	10.60 ± 5.90

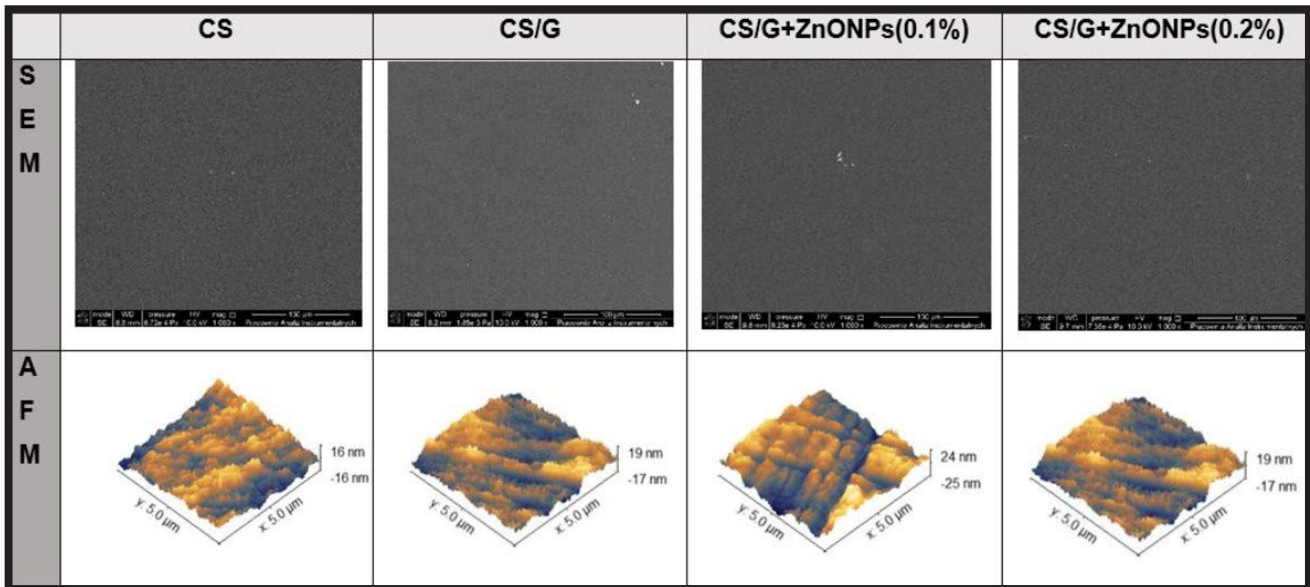


FIG. 4. SEM and AFM images of polymer films (SEM magnification 1000x).

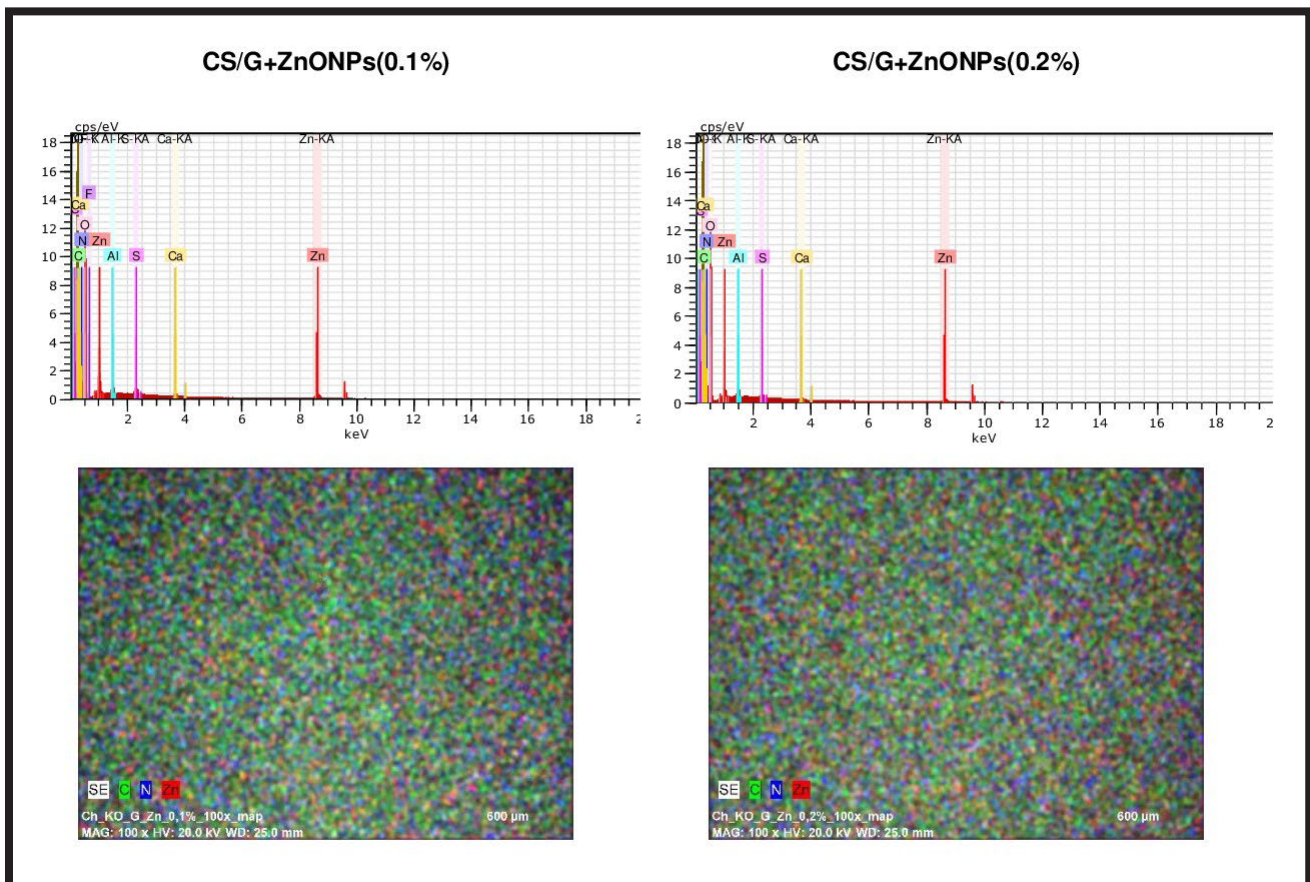


FIG. 5. Analysis (SEM-EDX) of the elemental composition of the samples with the addition of zinc oxide nanoparticles with mapping.

TABLE 3. Roughness parameters of chitosan films with and without additives.

Sample	CS	CS/G	CS/G+ZnONPs(0.1%)	CS/G+ZnONPs(0.2%)
$R_q$ [nm]	$4.80 \pm 1.13$	$6.85 \pm 0.46$	$7.06 \pm 0.67$	$4.45 \pm 0.56$
$R_a$ [nm]	$3.815 \pm 0.84$	$5.48 \pm 0.42$	$5.62 \pm 0.72$	$3.57 \pm 0.45$

**TABLE 4. Influence of chitosan films with the addition of various concentrations of ZnONPs on inhibition of test bacteria growth.**

Tested strain	Diameter of inhibition zone [mm ± SD]		
	CS/G	CS/G+ZnONPs(0.1%)	CS/G+ZnONPs(0.2%)
Staphylococcus aureus ATCC 25923	ND	ND	ND
Staphylococcus aureus ATCC 6538	ND	ND	ND
Salmonella infantis SES	ND	ND	ND
Salmonella enterica PCM 2565	ND	ND	ND
Pseudomonas aeruginosa ATCC 10145	ND	+	+
Listeria monocytogenes PCM 2191	ND	ND	ND
Escherichia coli ATCC 8739	ND	ND	ND
Escherichia coli ATCC 25922	ND	ND	ND
Klebsiella pneumoniae ATCC 700603	ND	ND	ND
Candida albicans ATCC 10231	ND	ND	ND

\*ND – antimicrobial activity not detected in the tested ZnONPs content in the film. +; growth inhibition

### Microbiological tests

The sensitivity of microorganisms to different contents of ZnONPs in the films was estimated by the inhibition growth zones under samples placed on inoculated agar plates. Results shown in TABLE 4 are the average of three separate experiments. The films with 0.1% and 0.2% content of ZnONPs showed antibacterial activity against *Pseudomonas aeruginosa* ATCC 10145. No antimicrobial activity has been observed against any of the other strains. Interestingly, Li et al. [37] found pure chitosan films to be active against bacteria of *Alicyclobacillus acidoterrestris*, *Staphylococcus aureus*, *Escherichia coli*, and *Salmonella* sp., which was in contrast to the findings of the present study. The authors also showed that antibacterial activity of the films increased with increasing content of ZnONPs (0.2, 0.4, and 0.6%). It was discussed that inhibition of bacterial growth of pure chitosan films resulted from antimicrobial properties of chitosan which forms porous structures on the surface of Gram-positive bacterial cells, binds to the cell membrane and disturbs its barrier function while in gram-negative bacteria chitosan penetrates into cells to adsorb its ionic substances and affects metabolism. These mechanisms could lead to the inhibition of bacterial growth. The additive of ZnONPs increased the antibacterial effect of chitosan films. In this case, ZnONPs enhance the positive charges of the chitosan amino group, which intensify interactions with the negatively charged bacterial cell walls. This may potentially exert a synergistic effect in ZnONPs composite films [37]. In the present study, the antibacterial effect of the nanocomposite films was not significant, but the ZnONPs content in the films was low. Zhang et al. [38] tested chitosan/ZnONPs films with different concentrations (0.1, 0.2, and 0.3%) and size (5, 50, and 100 µm) of ZnONPs for antibacterial activity against *Escherichia coli* and *Staphylococcus aureus*. The nanocomposite chitosan film containing 0.3% of 50 nm zinc oxide particles revealed the highest inhibition of bacterial growth indicating that smaller ZnONPs have better antibacterial activity. In the present study, ZnONPs had an irregular shape and showed an average size of  $117.79 \pm 4.71$  nm and a size ranging from 54.44 to 209.69 nm [31], which could affect lower penetration of nanoparticles into cells. However, the antibacterial activity of films with the additive of mycogenic ZnONPs against *Pseudomonas aeruginosa* strain is very promising, as the isolates of this species belong to ESKAPE pathogens, the multidrug resistant ones, and are one of the leading causes of the nosocomial infections throughout the world [39].

### Conclusions

The results of our research show that by adding zinc oxide nanoparticles (ZnONPs) to the chitosan solution, it is possible to obtain modified chitosan films in a simple way. The additives used in this research modify the properties of chitosan films. Spectrometric measurements confirmed changes in chitosan samples with the additive, resulting from interactions between the polymer and the nanoparticles. The addition of nanoparticles reduces the intensity of the bands and causes very slight shifts, which suggests a reduction in the number of intermolecular hydrogen bonds within the polymer matrix and the formation of new ZnONPs-chitosan hydrogen bonds. The Young modulus and tensile strength of the CS films increase when ZnONPs are added. To obtain films suitable for mechanical testing, the addition of a plasticizer was required. There was a slight change in the roughness parameters of the nanoparticle-enriched films compared to the pure chitosan film. All tested samples had a smooth surface morphology. The additives used allowed the properties of the films to be modified, particularly in terms of antimicrobial activity. The films show antibacterial activity against the *Pseudomonas aeruginosa* strain even at low concentrations of ZnONPs. This is a particularly desirable feature for topical application of this material on the skin. The proposed combination could potentially have applications in cosmetics and biomedical applications such as wound dressing.

### Acknowledgements

Statutory activity of KChBiK WCh UMK in Toruń.

### ORCID iD

K. Kulka: <https://orcid.org/0000-0002-0825-1774>  
A. Szejmowska: <https://orcid.org/0009-0001-8992-1214>  
A. Sionkowska: <https://orcid.org/0000-0002-1551-2725>  
M. Wypij: <https://orcid.org/0000-0002-1480-6094>  
P. Golińska: <https://orcid.org/0000-0001-9154-8191>

## References

- [1] Muthu M., Gopal J., Chun S., Devadoss A.J.P., Hasan N., Sivanesan I.: Crustacean waste-derived chitosan: Antioxidant properties and future perspectives. *Antioxidants* 10 (2021) 228.
- [2] Younes I., Rinaudo M.: Chitin and chitosan preparation from marine sources. Structure, properties and applications. *Marine Drugs* 13 (2015) 1133-1174.
- [3] Kulka K., Sionkowska A.: Chitosan Based Materials in Cosmetic Applications: A Review. *Molecules* 28 (2023) 1817.
- [4] Guzman E., Ortega F., Rubio R.G.: Chitosan: A Promising Multifunctional Cosmetic Ingredient for Skin and Hair Care. *Cosmetics* 9 (2022) 99.
- [5] Ferreira P.G., Ferreira V.F., Silva F., Freitas C.S., Pereira P.R., Paschoalin V.M.F.: Chitosans and Nanochitosans: Recent Advances in Skin Protection, Regeneration, and Repair. *Pharmaceutics* 14 (2022) 1307.
- [6] Sheokand B., Vays M., Kumar A., Srivastava C.M., Bahadur I., Pathak S.R.: Natural polymers used in the dressing materials for wound healing: Past, present and future. *Journal of Polymer Science* 61 (2023) 1389-1414.
- [7] Doderò A., Scarfi S., Mirata S., Sionkowska A., Vicini S., Alloisio M., Castellano M.: Effect of crosslinking type on the physical-chemical properties and biocompatibility of chitosan-based electrospun membranes. *Polymers* 13 (2021) 831.
- [8] Wahba M.I.: Enhancement of the mechanical properties of chitosan. *Journal of Biomaterials Science, Polymer Edition* 31 (2020) 350-357.
- [9] Machado A.H.S., Garcia I.M., Motta A., Leitune V.C.B., Collares F.M.: Triclosan-loaded chitosan as antibacterial agent for adhesive resin. *Journal of Dentistry* 83 (2019) 33-39.
- [10] Preethi S., Abarna K., Nithyasri M., Kishore P., Deepika K., Ranjithkumar R., Bhuvaneshwari V., Bharathi D.: Synthesis and characterization of chitosan/zinc oxide nanocomposite for antibacterial activity onto cotton fabrics and dye degradation applications. *International Journal of Biological Macromolecules* 164 (2020) 2779-2787.
- [11] Rajasekaran P., Santra S.: Hydrothermally treated chitosan hydrogel loaded with copper and zinc particles as a potential micro-nutrient - Based Antimicrobial Feed Additive. *Frontiers in Veterinary Science* 2 (2015) 62.
- [12] Zhang X., Ismail B.B., Cheng H., Jin T.Z., Qian M., Arabi S.A., Liu D., Guo M.: Emerging chitosan-essential oil films and coatings for food preservation – A review of advances and applications. *Carbohydrate Polymers* 273 (2021) 118616.
- [13] Lian R., Cao J., Jiang X., Rogachev A.V.: Physicochemical, antibacterial properties and cytocompatibility of starch/chitosan films incorporated with zinc oxide nanoparticles. *Materials Today Communications* 27 (2021) 102265.
- [14] Matatkova O., Michailidu J., Miskovska A., Kolouchova I., Masak J., Cejkova A.: Antimicrobial properties and applications of metal nanoparticles biosynthesized by green methods. *Biotechnology Advances* 58 (2022) 107905.
- [15] Khan I., Saeed K., Khan I.: Nanoparticles: Properties, applications and toxicities. *Arabian Journal of Chemistry* 12 (2019) 908-931.
- [16] Ahmed F., Prashanth S., Sindhu K., Nayak A., Chaturvedi S.: Antimicrobial efficacy of nanosilver and chitosan against *Streptococcus mutans*, as an ingredient of toothpaste formulation: An in vitro study. *Journal of Indian Society of Pedodontics and Preventive Dentistry* 37 (2019) 46-54.
- [17] Fatoni A., Yessica H.S., Aldilah, Almi M., Rendowaty A., Romsiah, Sirumapea L., Hidayati N.: The Film of Chitosan-ZnO Nanoparticles-CTAB: Synthesis, Characterization and In Vitro Study. *Science and Technology Indonesia* 7 (2021) 58-66.
- [18] Mujeeb Rahman P., Abdul Mujeeb V.M., Muraleedharan K., Thomas S.K.: Chitosan/nano ZnO composite films: Enhanced mechanical, antimicrobial and dielectric properties. *Arabian Journal of Chemistry* 11 (2018) 120-127.
- [19] Soubhagya A.S., Moorthi A., Prabakaran M.: Preparation and characterization of chitosan/pectin/ZnO porous films for wound healing. *International Journal of Biological Macromolecules* 157 (2020) 135-145.
- [20] Thomas V., Yallapu M.M., Sreedhar B., Bajpai S.K.: Fabrication, characterization of chitosan/nanosilver film and its potential antibacterial application. *Journal of Biomaterials Science, Polymer Edition* 20 (2009) 2129-2144.
- [21] Ali A., Phull A.R., Zia M.: Elemental zinc to zinc nanoparticles: Is ZnNPs crucial for life? Synthesis, toxicological and environmental concerns. *Nanotechnology Reviews* 7 (2018) 413-441.
- [22] Sharma P., Reddy P.K., Kumar B.: Trace Element Zinc, a Nature's Gift to Fight Unprecedented Global Pandemic COVID-19. *Biological Trace Element Research* 199 (2021) 3213-3221.
- [23] Skrajnowska D., Bobrowska-Korczak B.: Role of zinc in immune system and anti-cancer defense mechanisms. *Nutrients* 11 (2019) 2723.
- [24] Ginzburg A.L., Blackburn R.S., Santillan C., Trulong L., Tanguay R.L., Hutchison J.E.: Zinc oxide-induced changes to sunscreen ingredient efficacy and toxicity under UV irradiation. *Photochemical and Photobiological Sciences* 20 (2021) 1237-1285.
- [25] Cuajungco M.P., Ramirez M.S., Tolmasky M.E.: Zinc: Multidimensional effects on living organisms. *Biomedicines* 9 (2021) 1-25.
- [26] Slavin Y.N., Asnis J., Hafeli U.O., Bach H.: Metal nanoparticles: Understanding the mechanisms behind antibacterial activity. *Journal of Nanobiotechnology* 15 (2017) 65.
- [27] Czyżowska A., Barbasz A.: A review: zinc oxide nanoparticles – friends or enemies? *International Journal of Environmental Health Research* 32 (2022) 885-901.
- [28] Singh A., Singh N.Á., Afzal S., Singh T., Hussain I.: Zinc oxide nanoparticles: A review of their biological synthesis, antimicrobial activity, uptake, translocation and biotransformation in plants. *Journal of Materials Science* 53 (2018) 185-201.
- [29] Trzcińska-Wencel J., Wypij M., Terzyk A.P., Rai M., Golińska P.: Biofabrication of novel silver and zinc oxide nanoparticles from *Fusarium solani* IOR 825 and their potential application in agriculture as biocontrol agents of phytopathogens, and seed germination and seedling growth promoters. *Frontiers in Chemistry* 11 (2023) 1235437.
- [30] Bandeira M., Giovanela M., Roesch-Ely M., Devine D.M., Silva Crespo J.: Green synthesis of zinc oxide nanoparticles: A review of the synthesis methodology and mechanism of formation. *Sustainable Chemistry and Pharmacy* 15 (2020) 100223.
- [31] Mirzaei H., Darroudi M.: Zinc oxide nanoparticles: Biological synthesis and biomedical applications. *Ceramics International* 43 (2017) 907-914.
- [32] Liu H., Adhikari R., Adhikari B.: Preparation and characterization of glycerol plasticized (high-amylose) starch-chitosan films. *Journal of Food Engineering* 116 (2013) 588-597.
- [33] Jakubowska E., Gierszewska M., Szydłowska-Czerniak A., Nowaczyk J., Olewnik-Kruszkowska E.: Development and characterization of active packaging films based on chitosan, plasticizer, and quercetin for repassed oil storage. *Food Chemistry* 399 (2023) 135617.
- [34] Yin Y.J., Yao K.D., Cheng G.X., Ma J.B.: Properties of polyelectrolyte complex films of chitosan and gelatin. *Polymer International* 48 (1999) 429-433.
- [35] Khung K., Ibutoto Z.H., AlSalhi M.S., Atif M., Ansari A.A., Willander M.: Fabrication of Well-Aligned ZnO Nanorods Using a Composite Seed Layer of ZnO Nanoparticles and Chitosan Polymer. *Materials* 6 (2013) 4361-4374.
- [36] Dobrucka R., Dugaszewska J.: Biosynthesis and antibacterial activity of ZnO nanoparticles using *Trifolium pratense* flower extract. *Saudi Journal of Biological Sciences* 23 (2016) 517-523.
- [37] Li Y., Zhou Y., Wang Z., Cai R., Yue T., Cui L.: Preparation and Characterization of Chitosan-Nano-ZnO Composite Films for Preservation of Cherry Tomatoes. *Foods* 10 (2021) 3135.
- [38] Zhang X., Zhang Z., Wu W., Yang J., Yang Q.: Preparation and characterization of chitosan/Nano-ZnO composite film with antimicrobial activity. *Bioprocess Biosystems Engineering* 44 (2021) 1193-1199.
- [39] Santajit S., Indrawattana N.: Mechanisms of Antimicrobial Resistance in ESKAPE Pathogens. *Biomed Research International* 2016 (2016) 2475067.